Evaluation of the turbulent energy cascade rates from the upper inertial range in the solar wind at 1 AU

Bernard J. Vasquez,[1] Charles W. Smith,[1] Kathleen Hamilton,[1] Benjamin T. MacBride,[1] and Robert J. Leamon[2]

Received 27 January 2007; revised 16 March 2007; accepted 28 March 2007; published 7 July 2007.

[1] We construct a database from ACE spacecraft measurements of solar wind magnetic field fluctuations at 1 AU which resolves ~2 decades in frequency at the high end of the inertial range. Using magnetic field measurements outside of magnetic clouds in combination with plasma measurements, we evaluate expressions for the Kolmogorov and Kraichnan cascade rates at 0.01 Hz from magnetic field power spectra and consider both isotropic and cross-field rates. We examine these rates as functions of proton temperature and solar wind speed, comparing them to the expected rate based on the heating of protons at 1 AU. The average Kolmogorov rate is consistently more than a factor of 10 greater than expected. We conclude that the cascade rate cannot be estimated using the Kolmogorov prescription and power spectra. The Kraichnan rate is close to the expected rate and is potentially a good way to estimate the cascade rate. No distinction is found between the isotropic and cross-field rates at 1 AU. However, consideration of the likely dependence of cascade rates with distance from the Sun shows that a distinction should exist at distances closer than 1 AU but not outside 1 AU. Moreover, we find that inside 1 AU, the cross-field Kraichnan prediction can maintain agreement with the expected heating rate whereas the isotropic prediction cannot.

Citation: Vasquez, B. J., C. W. Smith, K. Hamilton, B. T. MacBride, and R. J. Leamon (2007), Evaluation of the turbulent energy cascade rates from the upper inertial range in the solar wind at 1 AU, *J. Geophys. Res.*, *112*, A07101, doi:10.1029/2007JA012305.

1. Introduction

[2] The solar corona is a hot $\sim 10^6$ K plasma where significant heat addition occurs. The additional heat is of such a large amount that the corona cannot be static and bounded by the gravitational potential of the Sun and is instead accelerated to supersonic and super-Alfvénic speeds away from the Sun (see review by *Velli* [2001] and references therein). The resulting solar wind can be classified as either fast (≥500 km/s) or slow (<500 km/s) [e.g., *Neugebauer and Snyder*, 1966; *McComas et al.*, 2000].

[3] With weaker intensity, heating and acceleration continues away from the Sun. The proton temperature has been measured as close as 0.3 AU from the Sun by Helios spacecraft [e.g., *Marsch et al.*, 1982, 1983; *Schwenn*, 1983; *Freeman*, 1988] and as far away as 100 AU or more by Pioneer and Voyager spacecraft [e.g., *Gazis*, 1984; *Gazis et al.*, 1994; *Richardson et al.*, 1995]. The combined database of measurements shows that the radial component of the proton temperature T_{pr} as a function of heliocentric distance r is not in accord with adiabatic cooling due to spherical expansion of the solar wind wherein $T_p \propto r^{-4/3}$. Instead, proton heating is found where $T_{pr} \propto r^{-0.9}$ [e.g., *Schwenn*, 1983; *Totten et al.*, 1995] between 0.3 and 1 AU and eventually flattens further to $T_{pr} \propto r^{-0.7}$ near 10 AU [e.g., *Gazis et al.*, 1994] where pickup ions contribute significantly and even increases with r beyond 30 AU [e.g., *Richardson et al.*, 1995; *Zank et al.*, 1996; *Smith et al.*, 2001a]. Heating near the Sun can be modeled by using a polytropic equation of state with a specific heat ratio of nearly unity [e.g., *Totten et al.*, 1995]. In MHD numerical simulations, polytropic approximations can well mimic the steady fast wind but do not capture the time-dependent character of slow wind. Such modeling also does not explain the source of the heating.

[4] Helios measurements from 0.3 to 1 AU contribute especially to detailing the nonthermal nature of solar wind protons and the addition of heat as they convect from 0.3 to 1 AU. Nearly radial alignment of the two Helios spacecraft allowed comparison of energy balance in particular streams as a function of distance [e.g., *Schwartz and Marsch*, 1983]. However, alignment occurred infrequently, and the average properties of many streams could not be obtained. Alternatively, a large amount of observations of T_{pr} are available at various distances from the Sun which can be combined into a statistically significant investigation. *Schwenn* [1983] made the first significant study to find the dependence of T_{pr} on r as a function of V_{SW} as it would occur in a spherically symmetric expanding solar wind. The proximity of slow and fast winds leads to compression where the fast wind overtakes the slow wind from behind and to expansion

[1]Space Science Center, University of New Hampshire, Durham, New Hampshire, USA.
[2]ADNET Systems, Inc., NASA Goddard Space Flight Center, Greenbelt, Maryland, USA.

Copyright 2007 by the American Geophysical Union.
0148-0227/07/2007JA012305

where the fast wind is ahead of the slow wind. This contributes about 15% of the net solar wind heating at 1 AU [e.g., *Burlaga and Ogilvie*, 1973; *Pizzo et al.*, 1973] averaged over a few solar rotations. This component can be removed by excluding intervals with stream interactions. The amount of heating then found can be more usefully compared to turbulent energy cascades. Data points are binned for average speeds between 300 and 800 km/s with each bin having a width of 100 km/s. The results show that fast winds tend to be heated significantly but the slowest winds at 300–400 km/s are almost adiabatic.

[5] *Lopez and Freeman* [1986] use similar methods to project Helios measurements between 0.3 and 1 AU to their values at 1 AU. The resulting distribution of T_{pr} as a function of V_{SW} is quite broad but shows two main populations separated at 500 km/s into slow and fast wind sets. With increasing speed, slow wind temperatures rise from $\sim 10^4$ to $\sim 10^5$ K with increasing V_{SW}. In fast wind the rate of increase in T_{pr} with V_{SW} is distinctly less than in slow wind and $T_{pr} \sim 10^5$ K.

[6] Protons in fast winds show increases in the magnetic moment where perpendicular proton temperature increases relative to adiabatic expectations [*Marsch et al.*, 1983] and specific entropy increases with r [*Marsch and Richter*, 1987]. However, these results, to a lesser degree, are also determined to be true for slow winds and so contradict the results of *Schwenn* [1983]. The heating of the slow wind finally becomes evident when corrections are made to the original Schwenn analysis by *Arya and Freeman* [1991], *Freeman et al.* [1992], and *Totten et al.* [1995]. *Arya and Freeman* [1991] find that slow winds experience a significant amount of acceleration between 0.3 to 1 AU relative to fast winds. The amount affects the process of sorting data points into solar wind speed bins. For example, winds of 300–400 km/s at 1 AU cannot be compared to winds of the same speed range at 0.3 AU but rather should be compared to slower ones. Additionally, a smaller correction due to the varying spacecraft orbital speed at various r means that locations especially near 0.3 AU are undersampled relative to 1 AU. This correction simply amounts to equalizing the weight given to all measurements in 0.1 AU bins over the interval between 0.3 and 1 AU. Once these corrections are made, slow and fast winds are found to be heated and have T_{pr} varying as $r^{-0.9 \pm 0.1}$ [*Freeman et al.*, 1992; *Totten et al.*, 1995].

[7] The processes governing the heating are potentially a mix of continued sources and mechanisms active in the corona and new ones active only further away from the Sun. Within a few AU of the Sun, the primary source of energy for in situ heating is believed to be the turbulent cascade among Alfvénic fluctuations [e.g., *Coleman*, 1968; *Matthaeus and Goldstein*, 1982; *Tu et al.*, 1984; *Hollweg*, 1986; *Tu*, 1988; *Zhou and Matthaeus*, 1990; *Smith et al.*, 2006c]. This is a view which will be pursued in this paper. The turbulence could be driven by the solar wind velocity shears and compressions observed at large scales, which are especially prevalent in the ecliptic plane. The stirring at these large scales can cause an energy cascade via nonlinear forces. Ultimately, the energy is dissipated at small scales where the plasma is heated. Only a small fraction of the total energy in solar wind speed gradients is needed to cause all the proton heating found in the solar wind between 0.3 and 1 AU. However, the required energy does exceed the amount of fluctuation power observed at the high end of the wave spectrum which could be damped when swept into cyclotron resonance with protons under the assumption that an energy cascade is not active [*Schwartz et al.*, 1981]. Presuming that some of the perpendicular proton heating requires waves to resonate with proton cyclotron frequencies or attain scales or frequencies to which protons no longer act adiabatically, then one can infer further that an active energy cascade is necessary to explain solar wind heating.

[8] In this paper we undertake an evaluation of turbulent cascade rates estimated from power spectra and determine their merit based on how their average values compare with expected heating rates. Section 2 explains the cascade rate predictions based on Kolmogorov and Kraichnan which are evaluated in this paper and gives new predictions for cross-field cascades. Section 3 discusses the expected heating rates for protons, alphas, and electrons, and outlines the method that we use to find the uncertainty from the equation of state in determining heating rates. Section 4 presents prior work on evaluations of the cascade rates. Section 5 describes our database and its properties. Section 6 gives our results for cascade rates. In section 7 we consider the likely behavior of cascade rates with distance from the Sun. Section 8 summarizes the results and conclusions.

2. Turbulent Cascade Rates

[9] Across a large intermediate range between the energy containing and dissipation scales in the solar wind, power in fluctuations is organized into an inertial range. At 1 AU, this inertial range extends from spacecraft frequencies of about 10^{-4} to 0.2 Hz. Observed magnetic field component power spectra are most often found to obey a dependence with frequency ν according to power laws which range mostly from $\nu^{-3/2}$, as predicted by *Kraichnan* [1965], to ones steeper than $\nu^{-5/3}$, as predicted by the extension of the *Kolmogorov* [1941] model to magnetohydrodynamics (MHD). On average, indices are closer to Kolmogorov values than Kraichnan [e.g., *Matthaeus and Goldstein*, 1982]. Structure functions [e.g., *Horbury et al.*, 1996; *Forman and Burlaga*, 2003; *MacBride et al.*, 2005] of the fluctuations have been examined and are most consistent with the Kolmogorov prediction. In the Kolmogorov prediction the third-order structure function is linear in lag, whereas in the Kraichnan the fourth-order structure function is linear. However, a recent work has shown that the magnetic field spectra may be steepened by the presence of abrupt magnetic field rotations, called directional discontinuities. *Borovsky* [2006] has found that magnetic field data taken between directional discontinuities with large spread angles give $\nu^{-3/2}$ spectra. *Podesta et al.* [2006] have determined the fluctuation velocity power spectrum to relatively high frequencies. They found that it is flatter than the magnetic field spectrum and closer to $\nu^{-3/2}$. There is then a possibility that the Kraichnan prediction could be valid for the solar wind turbulence.

[10] The rate of energy dissipation in hydrodynamic turbulence theory [*Kolmogorov*, 1941] is equal to the rate of energy cascade through the inertial range. The cascade is governed by the nonlinear turn-over time $\tau_{NL} = l/\delta V$ of

Table 1. Effect of Cross-Helicity on Cascade Rate[a]

σ_c	α_1	$\epsilon_{Kol,c}/\epsilon_{Kol}$	$\epsilon_{Kr,c}/\epsilon_{Kr}$
0.00	1.0000	1.0000	1.0000
0.05	0.9048	0.9984	0.9975
0.10	0.8182	0.9937	0.9900
0.15	0.7391	0.9859	0.9775
0.20	0.6667	0.9748	0.9600
0.25	0.6000	0.9605	0.9375
0.30	0.5385	0.9429	0.9100
0.35	0.4815	0.9218	0.8775
0.40	0.4286	0.8972	0.8400
0.45	0.3793	0.8688	0.7975
0.50	0.3334	0.8365	0.7500
0.55	0.2903	0.8000	0.6975
0.60	0.2500	0.7589	0.6400
0.65	0.2121	0.7129	0.5775
0.70	0.1765	0.6611	0.5100
0.75	0.1429	0.6029	0.4375
0.80	0.1111	0.5367	0.3600
0.85	0.0811	0.4603	0.2775
0.90	0.0526	0.3693	0.1900
0.95	0.0264	0.2529	0.0975
1.00	0.0000	0.0000	0.0000

[a]For the Kraichnan cascade, $\epsilon_{Kr,c}$ is calculated for $R_A = 0$ where it formally agrees with ϵ_{Kr} when $\sigma_c = 0$.

fluctuations where l is the length scale and δV is velocity amplitude of the fluctuation. Under the assumption of isotropic hydrodynamic turbulence, Kolmogorov used dimensional analysis to predict that the inertial range of the three-dimensional (3-D) omnidirectional spectrum of turbulent velocity fluctuations, $E_V(k)$, has the form:

$$E_V(k) = C_K \epsilon^{2/3} k^{-5/3} \tag{1}$$

where $\epsilon(\propto \delta V^3/l)$ is the energy cascade rate per unit mass, $k(= 2\pi/l)$ is wave number, and C_K is an order unity quantity for which $C_K \approx 1.6$ [e.g., *Sreenivasan*, 1995; *Yeung and Zhou*, 1997] as determined by hydrodynamic experiments. However, $E_V(k)$ is not what we measure with a single spacecraft. We measure $E_V(k_r) = E_V(\mathbf{k} \cdot \mathbf{V_{SW}})$ which is the reduced spectrum using the frozen-in-flux assumption recorded along the solar wind velocity. Assuming an isotropic spectrum of magnetic fluctuations, a consistent ratio of energy is associated with the velocity and magnetic fluctuations $R_A = E_V/E_B$ in the inertial range, a wind speed V_{SW}, and adopting $P_B(\nu)$ to be the measured magnetic spectrum as a function of frequency, we can write the 3-D omnidirectional cascade rate for kinetic and magnetic energy as [*Leamon et al.*, 1999]:

$$\epsilon_{Kol} = (2\pi/V_{SW})\nu^{5/2}\left[(1+R_A)(5/3)\left(P_B(\nu)/\mu_0 m_p n_p\right)/C_K\right]^{3/2}, \tag{2}$$

where m_p is the proton mass and n_p is the proton number density. This is the prediction which will be tested in this paper with an assumed value of $R_A = 1/2$ (see section 6) because velocity measurements are not available at the high frequencies. Additionally, the value of $C_K = 1.6$ is taken to be the one from hydrodynamic experiments. This is an assumption which is often used in analyses [e.g., *Matthaeus and Zhou*, 1989] and in comparable observational studies [e.g., *Leamon et al.*, 1999]. As discussed in more detail below, MHD turbulence is expected to cascade energy across the magnetic field where Alfvén waves do not propagate. In such circumstances the turbulent eddies might be more closely associated with hydrodynamic ones than with waves. The estimated interaction time to cascade the energy between hydrodynamic eddies is $C_K^{3/2}\tau_{NL}$ wherein we express ϵ as an energy per unit mass δV^2 divided by the interaction time. Thereby, $C_K = 1.6$ yields an interaction time near $2\tau_{NL}$. Values of C_K for MHD are expected to be of order unity so that the interaction time is near the value of $2\tau_{NL}$ as is found for hydrodynamics. However, the true value of C_K for MHD has not been definitively established. *Verma et al.* [1996] give the only published study of the value of C_K in 3-D MHD simulations, and they find the larger value $C_K = 3.6$.

[11] In MHD the nonlinear generalized Reynolds stresses that can drive turbulence require that the velocity and magnetic field fluctuations are not at 0 or 180° in phase, as it is for Alfvén waves with group velocity in one direction. This requirement can be assessed using the absolute value of the normalized cross-helicity σ_c where $\sigma_c \equiv |\delta\mathbf{V} \cdot \delta\mathbf{B}|/(\delta V \delta B)$. A particular prediction which depends on σ_c is derived by *Zhou and Matthaeus* [1990] and is given in terms of Elsässer variables $\mathbf{z}^\pm = \delta\mathbf{V} \pm \delta\mathbf{B}/(\mu_0 m_p n_p)^{1/2}$ and pseudoenergies $E^\pm = \mathbf{z}^\pm \cdot \mathbf{z}^\pm/2$. Cascade rates can be expressed as $\epsilon^\pm = C_K^{-3/2}[E^\pm(k)]\,[E^\mp(k)]^{1/2}\,k^{5/2}$ and the total rate is the average $(\epsilon^+ + \epsilon^-)/2$. The expression for the total rate can be related to (2) by

$$\epsilon_{Kol,c} = \frac{\alpha_1 + \sqrt{\alpha_1}}{2}\left(\frac{2}{1+\alpha_1}\right)^{3/2}\epsilon_{Kol} \tag{3}$$

where $\alpha_1 = \min(E^-, E^+)/\max(E^-, E^+) = (1-\sigma_c)/(1+\sigma_c)$ is an Elsässer ratio which is restricted to the range 0 to 1. The ratio $\epsilon_{Kol,c}/\epsilon_{Kol}$ is tabulated in Table 1 as a function of α_1 and σ_c for convenient conversion between ϵ_{Kol} and $\epsilon_{Kol,c}$. Table 1 shows that for $\sigma_c < 0.8$, $\epsilon_{Kol,c} > \epsilon_{Kol}/2$. In our data and at the low-frequency end of the inertial range, $\sigma_c \approx 0.4$, so that the two predictions on average would be expected to be similar.

[12] The Kraichnan (or Iroshnikov-Kraichnan) cascade is based on a cascade time $lV_A/(\delta\mathbf{V} \cdot \delta\mathbf{V})$, where V_A is the Alfvén speed, from a large number of uncorrelated interactions between oppositely propagating Alfvén waves [*Iroshnikov*, 1964; *Kraichnan*, 1965]. Fluctuation kinetic and magnetic energy are assumed to be equipartitioned ($R_A = 1$). Here the power spectrum has a $-3/2$ spectral index. The 3-D omnidirectional cascade rate can be expressed in terms of the magnetic spectrum as [*Leamon et al.*, 1999]

$$\epsilon_{Kr} = (2\pi/V_{SW})V_A^{-1}\nu^3\left[(3/2)\left(P_B(\nu)/\mu_0 m_p n_p\right)/A\right]^2. \tag{4}$$

In the Kraichnan prediction the cascade rate is not dependent on the sum of the kinetic and magnetic energy but rather on either one of them individually, presuming energy equipartition. The value of A can be any order of unity constant and independent of C_K. However, in our work, we take $A = C_K^{3/4}$ so that $A = 1.42$ when $C_K = 1.6$. This relationship is found in the theory developed by *Matthaeus and Zhou* [1989]. In that work they assumed that the inverse

timescale for the decay of triple correlations is a sum of τ_{NL}^{-1} and the inverse Alfvén crossing time l/V_A. The resulting cascade is found to be a composite of both Kolmogorov and Kraichnan. In the weak magnetic field limit ($V_A \to 0$), a Kolmogorov cascade is recovered whereas for the strong field limit ($V_A \to \infty$), a Kraichnan cascade is found. In this paper we only consider the extremes of this prediction. In section 6 we will find that our data corresponds to the strong field limit so that the Kraichnan prediction should correspond closely to the value of ϵ found using the more general expression in the work of *Matthaeus and Zhou* [1989].

[13] From (2) and (4) the formal relationship between ϵ_{Kr} and ϵ_{Kol} can be expressed as

$$\epsilon_{Kr} = 0.457\left(\frac{V_{SW}}{2\pi}\right)^{1/3}\frac{\nu^{-1/3}}{V_A}\epsilon_{Kol}^{4/3}, \tag{5}$$

where constants are evaluated as discussed earlier. Because $\epsilon_{Kr} \propto \epsilon_{Kol}^{4/3}$, whatever functional dependence ϵ_{Kol} has with temperature or solar wind speed, ϵ_{Kr} will tend to show a stronger dependence. The Kraichnan cascade rate for $|\delta\mathbf{V}|/V_A \ll 1$ is smaller than the corresponding Kolmogorov rate because nonlinear interactions based on propagation effects are relatively slow.

[14] *Dobrowolny et al.* [1980] derived a prediction which depends on the cross-helicity and can be expressed as

$$\epsilon_{Kr,c} = \alpha_1\left(\frac{2}{1+\alpha_1}\right)^2(1+R_A)^2\,\epsilon_{Kr}. \tag{6}$$

Equation (6) agrees formally with (4) in the limit of zero cross-helicity (i.e., $\alpha_1 = 1$) and zero kinetic energy ($R_A = 0$). In reality the two predictions are different since this agreement should have occurred when $R_A = 1$, which is the assumption in the Kraichnan prediction. The Dobrowolny et al. prediction depends on the sum of the kinetic and magnetic energy, as does the MHD extended Kolmogorov prediction, whereas the Kraichnan prediction does not. For $R_A = 0$, Table 1 shows that for $\sigma_c < 0.7$, $\epsilon_{Kr,c} > \epsilon_{Kr}/2$. If $R_A = 1/2$, as is assumed for evaluating the Kolmogorov prediction, then the factors in Table 1 for $\epsilon_{Kr,c}/\epsilon_{Kr}$ should be multiplied by 2.25. Again, in our data and at the low end of the inertial range, $\sigma_c \approx 0.4$, so that the two predictions on average would be expected to be similar for $R_A = 0$ but differ by a factor of about 2 for $R_A = 1/2$.

[15] Analysis and simulations based on MHD equations also show that the turbulent cascades are mostly in the direction perpendicular to the background magnetic field and produce smaller perpendicular scales [e.g., *Shebalin et al.*, 1983; *Oughton et al.*, 1994; *Matthaeus et al.*, 1996; *Ghosh et al.*, 1998a, 1998b; *Kinney and MacWilliams*, 1998; *Cho and Vishniac*, 2000; *Galtier et al.*, 2000, 2002; *Bhattacharjee and Ng*, 2001; *Dmitruk et al.*, 2002; *Cho et al.*, 2002; *Lithwick and Goldreich*, 2003; *Ng et al.*, 2003; *Oughton et al.*, 2003; *Beresnyak and Lazarian*, 2006]. Where fluctuations have wave vectors predominately across the magnetic field, the Alfvén time $\tau_A (= l_\parallel/V_A$ where $l_\parallel$ is the length scale of a fluctuation parallel to background magnetic field) can be small compared to τ_{NL}. In weak turbulence, where perturbation theory is valid, this can modify the isotropic Kraichnan cascade to form a perpendicular one where spectra obey $k_\perp^{-2}$ in the inertial range [e.g., *Bhattacharjee and Ng*, 2001]. However, in strong turbulence, which is expected for the solar wind, a Kolmogorov prediction $k_\perp^{-5/3}$ is found [e.g., *Goldreich and Sridhar*, 1995], assuming $\tau_{NL} \sim \tau_A$ and isotropy of scales in the perpendicular direction. Some 3-D simulation studies [e.g, *Matthaeus et al.*, 1996; *Verma et al.*, 1996; *Müller and Biskamp*, 2000; *Biskamp and Müller*, 2000; *Cho and Vishniac*, 2000; *Cho et al.*, 2002; *Cho and Lazarian*, 2003; *Haugen et al.*, 2004] find Kolmogorov cascades in the perpendicular direction. However, 2-D simulations [e.g., *Biskamp and Welter*, 1989; *Biskamp and Schwarz*, 2001; *Hyesook et al.*, 2003; *Ng et al.*, 2003] and other 3-D simulations [e.g., *Maron and Goldreich*, 2001; *Müller et al.*, 2003; *Müller and Grappin*, 2005] show that the turbulent cascade in the perpendicular direction can have $k_\perp^{-3/2}$ and Kraichnan cascade rates in the strong limit of turbulence. *Müller et al.* [2003] and *Müller and Grappin* [2005] conclude that the difference between 3-D simulation results is due to the moderating effect of the external and uniform background magnetic intensity B_{0e} relative to fluctuations. When $B_{0e}/|\delta\mathbf{B}| \lesssim 1$, a Kolmogorov cascade is found whereas when $B_{0e}/|\delta\mathbf{B}| = 5$ and 10, a Kraichnan cascade is found. The influence of B_{0e} then produces a composite of Kolmogorov and Kraichnan cascades, which reminds one of the *Matthaeus and Zhou* [1989] model for the isotropic case. *Boldyrev* [2005, 2006] explains the simulation results of Kraichnan cascades as arising in driven turbulence where the generation of current sheets results in a reduction of the nonlinearity by nearly aligning velocity and magnetic field fluctuations. The sheets are proposed to develop a localized anisotropy in the perpendicular direction where the smallest perpendicular length scale is across the current sheet and the other perpendicular scale is considerably larger due to significant advection. With such local scales, analysis of the cascade rate shows that the alignment possesses a nonzero minimum from which the Kraichnan prediction is obtained.

[16] With wave vector anisotropy, there is a projection effect between the inferred wave vector in the solar wind, which is in the radial direction, and corresponding wave vectors perpendicular to the background magnetic field. To find the amount of this effect, we first rewrite $P_B(\nu)$ in (2) as $\delta B^2\nu_0^{2/3}\nu^{-5/3}$ where δB^2 is the magnetic fluctuation amplitude squared at frequency ν_0. Then, ϵ_{Kol} can be shown to be proportional to the radial wave number $2\pi\nu_0/V_{SW}$. The corresponding projection of wave vectors from the 2-D spectrum has a wave number which is larger by the factor $1/|\sin\psi|$ where ψ is the angle between the background magnetic field and radial direction. Finally, there is a different constant in converting from a power spectrum which is confined in the two-dimensional (2-D) plane perpendicular to the background magnetic field into the observed reduced power spectrum. The formula for the 2-D Kolmogorov cascade rate $\epsilon_{Kol,\,2D}$ is derived in Appendix A and can be shown to be related to the isotropic form by

$$\epsilon_{Kol,2D} = \frac{0.772}{|\sin\psi|}\epsilon_{Kol}. \tag{7}$$

As with the Kolmogorov rate, the 2-D Kraichnan cascade rate $\epsilon_{Kr,2D}$ (see Appendix A) can similarly be shown to be

$$\epsilon_{Kr,2D} = \frac{0.764}{|\sin\psi|}\epsilon_{Kr}. \tag{8}$$

We believe that this is the first time that this form of the cascade rate in terms of the observed reduced spectrum has been derived and considered in a publication. A prediction dependent upon σ_c could also be made in (7) and (8) by replacing ϵ_{Kol} with $\epsilon_{Kol,c}$ and ϵ_{Kr} with $\epsilon_{Kr,c}$, respectively. Because ψ is mostly greater than 45° at 1 AU, the difference between the isotropic and 2-D forms will often be small. We thereby anticipate that no distinction between these forms will be identified at 1 AU in our data set. However, (7) and (8) should give a distinct prediction if applied to data well inside of 1 AU (see section 7).

3. Heating and Dissipation Rates

[17] In a steady state the cascade rate will equal the rate of dissipation and heat addition to the background plasma. Spherical expansion of the solar wind provides a means of cooling the plasma. *Verma et al.* [1995] derive an expression that combines in situ heating and adiabatic cooling in a spherical symmetric solar wind which we rewrite as:

$$\frac{dT_{pr}}{dr} + \frac{4}{3}\frac{T_{pr}}{r} = \frac{m_p}{(3/2)V_{SW}k_B}\epsilon \tag{9}$$

where T_{pr} is the radial component of the proton temperature, ϵ is a cascade rate, m_p is the proton mass, and k_B is the Boltzmann constant. All heating is assumed to go to the protons and the plasma mass per unit mole is approximated as that of protons alone. Since $T_{pr} = T_{pr,0}\,(r_0/r)^{\xi}$, we can solve (9) for ϵ at $r = r_0$ so that

$$\epsilon = \left(\frac{4}{3} - \xi\right)\frac{3}{2}\frac{V_{SW}}{r_0}\frac{k_B T_{pr,0}}{m_p}. \tag{10}$$

Substituting the stream average value $\xi = 0.9$ into (10) and evaluating constants for 1 AU, we can express the expected heating rate ϵ_{heat}, which accounts for proton heating, as

$$\epsilon_{heat} = 3.6 \times 10^{-5} T_{pr} V_{SW}\ [\mathrm{J/(kg\,s)}], \tag{11}$$

where T_{pr} has units K, and V_{SW} in km/s. The value of ϵ_{heat} will form an important part of our study to compare with rates obtained from power spectra. For typical solar wind values at 1 AU, the expected heating rate ranges from 10^2 J/(kg s) in cold wind to 10^4 J/(kg s) in hot wind. For a fixed T_{pr}, ϵ_{heat} varies only by a factor of 3 based on the observed range of V_{SW}. Cascade rates estimated from the energy-containing scale of turbulence at 1 AU by evaluating the triple-products of fluctuation magnetic fields and velocities and the correlation length scale of the turbulence also give values in this range [e.g., *Smith et al.*, 2001a, 2006c; *Isenberg*, 2005].

[18] In (9), proton pressure has been taken to be isotropic, so that T_{pr} has been assumed to correspond to the average temperature of parallel and perpendicular components in the studies of *Schwenn* [1983] and follow-on investigations. The preferential heating of protons is in the perpendicular direction and could be associated with the damping of proton cyclotron resonant waves [e.g., *Goldstein et al.*, 1994; *Leamon et al.*, 1998a, 1998b]. *Marsch et al.* [1983] used Helios data between 0.3 and 1 AU to show that the magnetic moment increases by 100% on average for both slow and fast solar wind streams. From here, we find that the rate of added thermal energy is 0.55 $V_{SW}B_0 d\mu/dr$ in J/(kg s), where B_0 is the background magnetic field strength in units of nT, V_{SW} is in units of km/s, and $d\mu/dr$ is the change of magnetic moment $T_\perp/B_0$ with r in units of 10^4 K/(AU · nT). For typical values at 1 AU, the rate of perpendicular heating falls into the same range as reported above from (11).

[19] In our study, only T_{pr} is available. The better measure of the overall energization of protons comes from the average proton temperature $T_p = (T_\parallel + 2T_\perp)/3$. We will first consider how the average temperature evolves and then how to relate the radial and average temperature. The average temperature T_j for any species j is taken from the trace of the gyrotropic pressure tensor $\mathbf{P}_j = n_j\,(T_{j\perp}\mathbf{I} + (T_{j\parallel} - T_{j\perp})\hat{\mathbf{b}}\hat{\mathbf{b}})$ for species j whose averaged trace is denoted by $P_j = n_j T_j$. The second peculiar velocity moment of the Boltzmann equation for each species gives the equation of state [e.g., *Barakat and Schunk*, 1982] which we express as

$$\left(\frac{\partial}{\partial t} + \mathbf{U}_j\cdot\nabla\right)\frac{3}{2}P_j = -\frac{5}{2}P_j\nabla\cdot\mathbf{U}_j - \left(\mathbf{P}_j - P_j\mathbf{I}\right):\nabla\mathbf{U}_j - \nabla\cdot\mathbf{q}_{j\parallel} + \rho\epsilon f_j \tag{12}$$

where $\mathbf{U}_j$ is the bulk velocity of species j, $q_{j\parallel}$ is the heat flux vector parallel to the magnetic field, $\rho = \sum_j n_j m_j$ is the total plasma mass density, f_j is the fraction of the total turbulent cascade energy that heats species j where $\sum_j f_j = 1$. In (12), the convected rate of change of internal energy is equated to the sum of adiabatic change and heat addition both from the divergence of parallel heat flux and from the turbulent energy cascade defined as $\rho\epsilon f_j$. Since the trace of $\mathbf{P}_j$ is taken, terms dependent on the energy exchanges between temperature components are eliminated. We have neglected the perpendicular component of heat flux which in the particular case of protons tends to be a factor 10 smaller than the parallel component [e.g., *Feldman et al.*, 1973]. Also, we have neglected Coulomb collisions which often give little energy rate change in the solar wind, energy exchange between species, and added heat from deceleration of differential streaming. We will examine the adequacies of these assumptions later.

[20] We first consider the proton equation of state. Choosing from a large set of data, we expect to average away terms dependent on time and on gradients in spherical polar coordinates ϕ and θ so that a radial and time-stationary equation of state remains. The position of ACE is such that results should average to those for $\theta = 90°$ and so only magnetic field and velocities in the $r\phi$ plane are kept. We further can make use of the equation of continuity with only the radial dependent gradients to replace density gradients with those of U_{pr} where $\partial\rho_p/\partial r = -2\rho_p/r - (\rho_p/U_{pr})(\partial U_{pr}/\partial r)$. The proton velocity distribution function can often be characterized as the sum of a beam (≈20% of total protons) and core where the beam streams

Table 2. Average Relative Uncertainties for Measurements and Analysis

Quantity	Relative Uncertainty
V_{SW}	2%
T_{pr}	27%
ϵ_{heat} equation (11)	50%
ϵ_{Kol} equation (2)	35%
ϵ_{Kr} equation (4)	39%
Whole analysis	68%

faster than the core along the background magnetic field. However, it is difficult to separate protons into completely distinct populations and eventually as the beam slows it becomes incorporated into the core. Therefore we consider the evolution of the protons without distinction. We then express the equation of state as a correction to (9)

$$\begin{aligned}\frac{3}{2}U_r k_B \frac{\partial T_p}{\partial r} &+ \frac{2U_r k_B T_p}{r} \\ &+ \frac{\partial U_r}{\partial r}\left(k_B T_p\right) + \left(\frac{\partial U_r}{\partial r} + \frac{2U_r}{r}\right)\left(\frac{(\mathcal{A}-1)}{1+2\mathcal{A}} k_B T_p\right) \\ &+ \left(\cos^2\psi \frac{\partial U_r}{\partial r} + \sin^2\psi \frac{U_r}{r}\right. \\ &\left. - \cos\psi \sin\psi \left(\frac{\partial U_{p\phi}}{\partial r} - \frac{U_{p\phi}}{r}\right)\right)\left(\frac{3k_B T_p(1-\mathcal{A})}{1+2\mathcal{A}}\right) \\ &- \frac{\cos\psi}{B}\frac{\partial B}{\partial r}\frac{q_{p\|}}{n_p} + \frac{\cos\psi}{n_p}\frac{\partial q_{p\|}}{\partial r} = \frac{\rho\epsilon}{n_p} f_p \end{aligned} \tag{13}$$

where $\mathcal{A} = T_\perp/T_\|$ is the total proton plasma anisotropy, and f_p is the fraction of the total turbulent cascade energy that heats protons (see *Krall and Trivelpiece* [1973, Appendix II] to obtain tensor components in spherical polar coordinates for (12)). The first two terms on the left-hand side of (13) correspond to those in (9). The remaining left-hand terms are additional ones dependent on acceleration, nonradial flow, plasma anisotropy, and parallel heat flux.

[21] We do not have all of the measurements which are needed to evaluate (13). In Appendix B we detail our method of using statistics for the unavailable quantities in the solar wind and estimate how much results using (13) differ from those using (9). We then determine the range of uncertainty for the cascade rate in (11). The results compared to power spectra derived values of ϵ are reported in section 6. The upshot of the analysis is the estimates using (11) are good to within a factor of 1.3 based on this uncertainty alone. The primary correction is due to the plasma anisotropy difference because $1 - \mathcal{A}$ multiplies a comparable term to that in (9). To show this, we can then reexpress (13) as

$$\begin{aligned}\frac{3}{2}V_{SW} k_B \frac{\partial T_p}{\partial r} &+ \frac{2V_{SW} k_B T_p}{r}\left(1 - \left(\cos^2\psi - \frac{1}{2}\sin^2\psi\right)\frac{1-\mathcal{A}}{1+2\mathcal{A}}\right) \\ &+ \text{other small terms} = \frac{\rho\epsilon}{n_p} f_p. \end{aligned} \tag{14}$$

The average value of $\mathcal{A}$ is 0.7 so that $(1 - \mathcal{A})/(1 + 2\mathcal{A}) = 0.125$. However, the trigonometric part of the shown terms in (14) changes sign and also vanishes at $\psi = 54.74°$ because this value of ψ satisfies $\tan^2\psi = 2$. This value of ψ is also near the average $\psi = 58°$ of our data. Thereby, we can see that at 1 AU, conditions are such that all correction terms are relatively small when we ensemble average the data.

[22] The radial component of temperature T_{pr} can be averaged for $\theta = 90°$ so that $T_{pr} = T_\| \cos^2\psi + T_\perp \sin^2\psi$. Since T_{pr} is measured, we relate this to T_p by

$$T_p = T_{pr}\frac{1+2\mathcal{A}}{3\left(\cos^2\psi + \mathcal{A}\sin^2\psi\right)}. \tag{15}$$

where $\psi = 54.74°$, $T_p = T_{pr}$ for all $\mathcal{A}$. In our data we can expect that on average T_p will be near T_{pr}. However, there is another important correction in the upward direction. Using the methods described in Appendix B, we will find in section 6 that the change of T_p with r on average is characterized by a smaller power law index ξ_{avg} with a value of 0.75. The importance of this difference comes not with respect to $\xi = 0.9$ but in the increased differential between the adiabatic index 4/3 and ξ_{avg}. This effect increases ϵ_{heat} by 22%. In section 6 we estimate that the overall relative uncertainty from the equation of state amounts to 50%. Additional uncertainties will come from the ϵ obtained from power spectra which has an average relative uncertainty of 37% and from matching this value to the proper value of ϵ_{heat} because the measured value of T_{pr} itself has an average relative uncertainty of 27%. The total relative uncertainty in the whole analysis is about 68%, and we will be satisfied if the value of ϵ from power spectra is within a factor of 2 of ϵ_{heat}. Table 2 summarizes the relative uncertainties encountered in this study.

[23] When the left-hand side of (13) is evaluated, the value of $f_p\epsilon$ which is then found will include the net effect of all external sources of energization in addition to turbulence. For instance, waves generated from microinstabilities can then damp on protons. Energy from these waves can come from other species but also from proton differential streaming between the beam and core. *Daughton and Gary* [1998] have shown that two populations with drifting bi-Maxwellian velocity distributions are unstable to mostly oblique waves when the drift exceeds a threshold speed above V_A. *Kaghashvili et al.* [2004] have shown that the presence of large-amplitude Alfvén waves enhances the instability. These studies demonstrate that such streaming instabilities are possible, but in the solar wind, the beam-core populations are not so distinct and the beam is more in the form of a plateau. This configuration undoubtedly reduces the energization of unstable waves compared to drifting biMaxwellians. The energy input from the damping of waves in a proton temperature anisotropy microinstability need not be considered because this case is eliminated by using the average temperature. Thereby, how well the estimated value of ϵ corresponds to the rate of turbulent energy cascade from large scales depends on the magnitude of other energy sources. The case of other species is detailed below. First, we examine differential streaming between beam and core proton populations.

[24] The beam proton population averages at a differential speed $V_{pp} \approx V_A$ and a relative concentration $n_b/n_p = 0.2$

[e.g., *Marsch et al.*, 1982]. To remain near the local value of V_A, the beam must decelerate at nearly the same rate that V_A decreases with increasing r. In fact, deceleration occurs somewhat faster and even for an azimuthal magnetic field where V_A can be constant. When combined with the core, much of the beam energy becomes part of the thermal energy and the speed along the magnetic field is then $(n_b/n_p)V_{pp}$. We estimate the loss of streaming energy $n_p\, m_p\, S$, where S is the rate per unit mass by

$$S = V_{SW}\left(0.1 + \cos^2\psi\right)\left(\frac{n_b}{n_p}\right)^2 \frac{V_{pp}^2}{r}. \tag{16}$$

Using typical solar wind values at 1 AU, S will be shown in section 6 to be mostly 30% or less than the heating rate. Some of this lost energy could go into increasing the core speed along the magnetic field and so the estimated value of S is an upper limit on what could be contributed to the thermal energy of protons. Some of the lost energy could go to waves in the dissipation range of wave numbers where they dissipate on protons, contributing to the heating rate but not to power spectra estimates of the cascade. Some of the lost energy could also go to waves in the high end of the inertial range and even participate in the energy cascade. In this case the rate of energy cascade at the high end could differ from the low end due to an input of wave energy at small scales. In any event, we have estimated that the rate of this input is small enough so that the majority of energy heating the protons should come from the turbulent energy cascade at large scales.

[25] From the right-hand side of (13), there is a certain amount of energy density $\rho\epsilon$ from the turbulent cascade which then must be dissipated among species according to $\rho\epsilon f_j/n_j$. The contribution of any species f_j to dissipating the turbulent cascade is approximately proportional to its relative concentration n_j/n_p. Most ions in the solar wind have such small relative concentrations that they can be neglected. The only significant ion species beyond protons are alphas. The relative concentration of alphas n_α/n_p averages about 4% [e.g., *Neugebauer*, 1981], and they have 4 times the mass of the protons. They give the only significant contribution to ρ. Alphas also typically stream faster than protons along the magnetic field. The alpha temperature T_α is about 2 times greater than T_p in slow winds and more than 4 times in fast winds. If we assume that the alpha temperature gradient is the same as the protons and disregard differential streaming, one can get a rough estimate of the contribution of alphas by multiplying (11) by (T_α/T_p) (n_α/n_p). Such estimates show that alphas on average are limited to a fraction (12–16%) of the energy dissipated by protons. In fast winds, where the average n_α/n_p and T_α are highest, the energetics of alphas have been shown by *Reisenfeld et al.* [2001] to be governed mostly by the loss of differential streaming energy into its own thermal energy. Thereby, the estimate discussed above is only an upper limit in the case of fast winds.

[26] We can neglect energy exchange between alphas and protons. Coulomb collisions under solar wind conditions provide a relatively small rate of energy change between alphas and protons. Lost streaming energy from alphas remains mostly with alphas. We conclude that if agreement between proton heating and turbulent cascade rates can only be estimated to within a factor of 2 using (11), then the alpha heating and energy exchange with protons can be neglected.

[27] Electrons have a relative concentration greater than protons such that $n_e = n_p + 2n_\alpha$ in accord with quasi-neutrality on scales much greater than the Debye length. They can potentially compete with protons in dissipating a turbulent cascade. The relative amount of proton to electron heating will vary with the particular wave modes and processes that occur in the dissipation range but at present these particulars are not well understood. *Leamon et al.* [1999] considered the damping of ion-cyclotron waves in an isotropic wave vector spectrum and found that proton and electron heating would be roughly equal in this case. If the modes are mostly confined to perpendicular directions, then these might be described as kinetic Alfvén waves which can be damped mostly at the Landau resonance and for electron greater than proton temperature mostly on electrons. *Leamon et al.* [1998b] used observations in the dissipation range of magnetic field helicity and the assumption of mostly outward propagation to estimate that 2/3 of the heating goes to cyclotron resonant damping, which is most likely heat addition to ions, and the remaining 1/3 to damping at the Landau resonance which should include heating of electrons.

[28] Observations of electron velocity distributions and moments show that their evolution is governed in a much different way than protons. First, it was noted that at 1 AU the average electron temperature near 1.4×10^5 K is independent of V_{SW} [e.g., *Newbury et al.*, 1998]. On the other hand, T_p tends to increase with V_{SW}, is highly variable within streams, and is typically hotter than electron temperature in the fastest winds. This has been interpreted as an indication that the turbulent cascade is primarily dissipated on protons rather than electrons (see *Hollweg* [1981] for a review of these ideas). Second, detailed observations of electrons have been carried out. Electrons have a two component velocity space distribution in the solar wind [e.g., *Feldman et al.*, 1975] consisting of a core and halo. (A third component, a strahl, consists of beamed halo electrons streaming along the magnetic field, but here we do not distinguish strahl from the overall halo.) These components can originate in the solar wind rather than in the corona [e.g., *Lie-Svendsen and Leer*, 2000]. The core is relatively isotropized by Coulomb collisions between other electrons and especially ions [e.g., *Phillips et al.*, 1989; *Phillips and Gosling*, 1990]. Although the angular distribution of electrons is strongly affected by ions, there is little exchange of energy between electrons and ions, which justifies the neglect of this effect in (13). The halo electrons are relatively collision free at their high velocities and carry much of the total heat flux in the solar wind which is directed away from the Sun [e.g., *Scime et al.*, 1994]. This heat flux is mostly due to the halo streaming on average faster than the core. In the core the heat flux is about 20% of the halo and directed toward the Sun. The halo has been found to account for much of the core heating so that external heat sources, as from a turbulent cascade, are relatively small contributors (but see *Pilipp et al.* [1990] for an alternative view in the case of fast winds). From all the above, we conclude that electron heating from a

turbulent cascade can be neglected in comparison to that of proton heating to within a factor of 2.

[29] Since we find no other species beyond protons to dissipate a significant portion of the turbulent cascade energy, we will always take $f_p = 1$ when evaluating (13) as we have already done in (11). Of course, the cascade rate estimated from power spectra will be made in an independent way, and so one is free to reconsider whether $f_p \approx 1$ or considerably smaller.

4. Comparison of Cascade and Heating Rates Using Power Spectra

[30] *Verma et al.* [1995] used OMNI-tape from spacecraft data at 1 AU which has a cadence of 1 hour. By this means, only the low-frequency end of the inertial range of fluctuations could be examined but both fluctuation magnetic field and velocity data were available. They distinguished non-Alfvénic ($\alpha_1 \approx 1$) from Alfvénic ($\alpha_1 = 0.07$) streams [e.g., *Roberts et al.*, 1987a, 1987b] and chose six streams during the years 1975–1976 near solar minimum based on uniform background properties for their investigation. Isotropic cascade rates with a cross-helicity dependence given by (3) and (6) were evaluated for each stream. Then a nearly equivalent expression of (9) was solved using the expected heating rate with parameters and amplitudes varying with r as appropriate to the stream studied. They fitted the data treating C_K and A as free parameters to match the average trends of proton temperature with r. For non-Alfvénic streams, they concluded that the Kolmogorov prediction gives a cascade rate consistent with expected heating for $C_K = 1$. For Alfvénic streams the rates were far too high and required $C_K = 8$ [see also *Tu*, 1988]. As such, results from non-Alfvénic and Alfvénic streams are in conflict with each other because Alfvénic ones would be expected to have lower rates of cascade as compared to non-Alfvénic ones. The Kraichnan rates were evaluated for $A = 0.5$ and 1.0. For no stream could the Kraichnan rates consistently match T_{pr} behavior simultaneously both inside and outside of 1 AU with the same value of A.

[31] *Leamon et al.* [1998a, 1998b, 1999] built a database of 32 one-hour intervals outside of magnetic clouds, referred to as open field intervals, to examine the high end of the inertial range and the dissipation range. Data were obtained from the Wind spacecraft at 1 AU. Development at the high end of the inertial range should approach the statistical equilibrium of the energy cascade faster than at the lower end and so may be a better place to evaluate cascade rates. Moreover, if there are sources of energy to the cascade from small scales, this can only be found by examining the high end. *Leamon et al.* [1999] used (2) and (4) and discussed only one interval. They concluded that the Kolmogorov rate was comparable to the expected heating rate but that the Kraichnan rate was too small.

[32] *Hamilton et al.* [2005] and *Smith et al.* [2005, 2006a, 2006b] have constructed a much larger database of one to several hour intervals using the Advanced Composition Explorer (ACE) spacecraft at 1 AU. *Smith et al.* [2006a, 2006b] evaluated only ϵ_{Kol} but limited the comparison to magnetic field variance and dissipation spectral index. In this paper we use the open field intervals from this database to evaluate ϵ_{Kol} and ϵ_{Kr} from magnetic field and background plasma data and to compare with ϵ_{heat} as functions of T_{pr} and V_{SW}. The database also includes a large number of cloud intervals, but since these undergo more than spherical expansion and do not have known radial temperature trends, we have chosen to exclude them from this paper. The chosen data differ from that of *Verma et al.* [1995] in that the data (1) are not chosen in particular streams or according to uniform background conditions, (2) come from a time around solar maximum, (3) are in the high end of the inertial range, and (4) provide only fluctuation magnetic field measurements at this high end. Additionally, data are drawn from 526 intervals which are far more than in previous studies.

[33] Our evaluation of the cascade rates will give some outstanding differences from the conclusions of *Verma et al.* [1995]. We will find that the average ϵ_{Kol} is systematically too high by a factor of 10 or more which is the result reported for the Alfvénic intervals. Although we cannot ascertain the cross-helicity at the frequencies of measurement, lower frequencies correspond mostly to non-Alfvénic intervals. The Kraichnan rate will be close to the expected value. Consideration of the likely behavior of the cascade rates with r will show that the 2-D Kraichnan rate stays near the expected rate with r and is possibly applicable in the solar wind.

5. Our Database and Its Properties

[34] We use magnetic field and plasma observations recorded by the ACE spacecraft [*Smith et al.*, 1998; *McComas et al.*, 1998] while on orbit at L1 from 1998 through 2002. We have built a database using the spectra of magnetic fluctuations from 960 intervals of data including samples from the widest possible range of solar wind conditions.

[35] We work with samples that are typically 1 to several hours in length. We include magnetic cloud observations [*Burlaga*, 1995] that make up half the database (393 intervals taken from 28 distinct clouds) along with rarefaction intervals, observations behind shocks, slow and fast wind conditions, etc., that make up the remainder (567 events). When employing thermal proton data in this analysis the database is reduced to 352 (526) intervals for clouds (open field lines) due to data availability. In this paper we consider only the open field lines.

[36] We follow the same analysis method used by *Leamon et al.* [1998a] and *Smith et al.* [2001b, 2004, 2006a, 2006b]. The inertial range of the parallel and perpendicular magnetic fluctuation spectra are fit to power law forms with the fitting interval adjusted to match the region of the spectrum that is well-described by a power law. We fit the range from 8 mHz to 0.1 Hz with only minor adjustment. This typically represents the high-frequency end of the inertial range at 1 AU. Figure 1 shows a typical example from the database.

[37] Figure 2 shows the spectral index in the upper inertial range as a function of T_{pr}, and Figure 3 gives a histogram of the spectral index. The index is mostly found between -1.5 and -1.8. The distribution is approximately symmetric about the average, as reported by *Smith et al.* [2006a], at -1.63 ± 0.14 which is closer to the Kolmogorov value. *Matthaeus and Goldstein* [1982] examined a large set

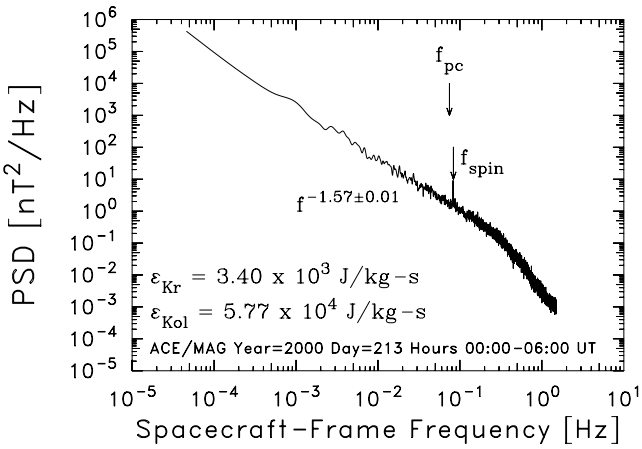

Figure 1. Example fluctuation magnetic field spectrum from the data base of 1 AU observations. The inertial range is well-fit by a −1.57 power law form. The break marking the onset of the dissipation range is visible. Positions of the proton cyclotron frequency f_{pc} and spacecraft spin frequency f_{spin} in the spacecraft frame are indicated with arrows. The computed values of ϵ_{Kol} and ϵ_{Kr} are given in the plot and are fairly typical of open field line observations at 1 AU.

of 1 AU data and showed that the average spectral index was near the Kolmogorov value. However, we do find a difference with the database used by *Leamon et al.* [1998a] because we see no tendency of the range of indices to narrow to one about an index between −3/2 and −5/3 at higher T_{pr}. Since our database is much larger, it is likely that Figure 2 better represents the actual solar wind. No theory

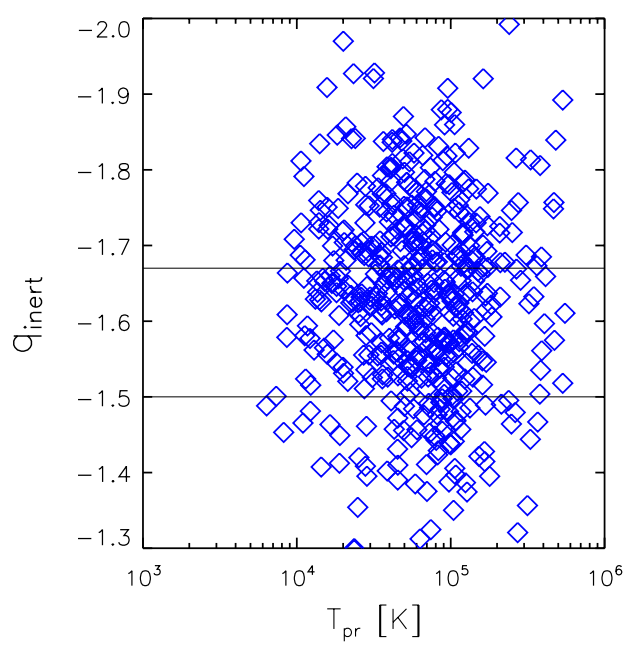

Figure 2. Scatterplot of the inertial range index q_{inert} as a function of the radial component of the proton temperature T_{pr}. Horizontal lines give the Kolmogorov (−1.67) and Kraichnan (−1.5) index values. At all T_{pr}, the index does not narrow around either Kolmogorov or the Kraichnan value.

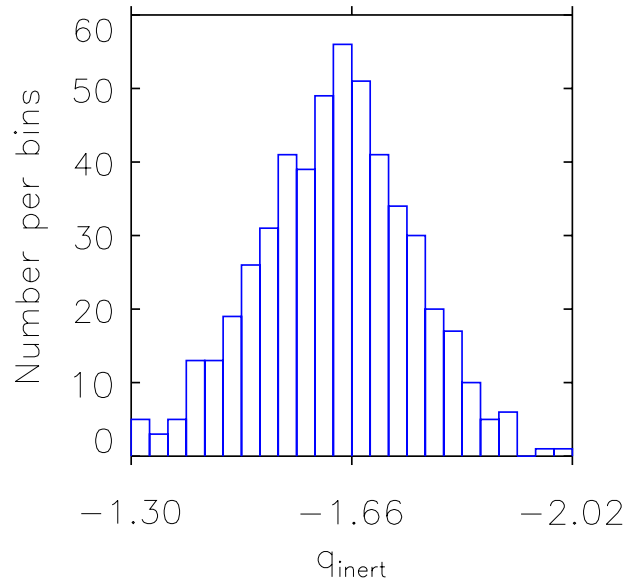

Figure 3. Histogram of q_{inert}. Average index is near the Kolmogorov value.

yet describes this range of indices, but it is in better agreement with Kolmogorov. However, in this paper we will consider the approaches of both Kolmogorov and Kraichnan in evaluating cascade rates. Behavior similar to Figure 2 is seen for the index as a function of V_{SW}, δB, and $\delta B/B_0$.

[38] The database was not constructed with regards to occurrence frequency in the solar wind nor was it made to sample intervals of solar wind speed in 100 km/s bins. Instead, the database most uniformly covers plasma conditions especially with regards to plasma β and so also n_p and T_{pr}. Before examining cascade rates, we need to assess how the database comports with overall solar wind behavior. We also highlight correlations with T_{pr} which will prove useful in our examination of cascade rates.

[39] Figure 4 plots T_{pr} as a function of V_{SW}. *Lopez and Freeman* [1986] showed that T_{pr} and V_{SW} fall into broad bands of slower than 500 km/s and greater than 500 km/s. We find that our data has a preponderance of slow wind data points. However, most of these points fall into the range of typical conditions. The break between temperature trends at 500 km/s is seen in the figure. We conclude from this that the data covers enough range of V_{SW} and T_{pr} so that typical heating rates should be found from (11).

[40] Figure 5 plots δB integrated over the 0.008 to 0.1 Hz spectral range as a function of T_{pr}. The fit line is made using the linear least squares method with unweighted uncertainties, since this will better suit our analysis of cascade rates in section 6, and has $\delta B = 3.35^{+2.51}_{-1.44} \times 10^{-3} T_{pr}^{0.46 \pm 0.05}$ [nT]. *Grappin et al.* [1990] evaluated daily average magnetic field fluctuation power and found a correspondingly similar dependence for total fluctuation energy in approximately the same frequency band examined here. The correlation has been interpreted to be of solar origin by *Grappin et al.* [1990] and *Smith et al.* [2006a]. Alternatively, *Bhattacharjee et al.* [2006] has suggested that the correlation might possibly result from pressure-driven interchange instability of background magnetic flux tubes at larger scales. A similar correlation is also observed for $\delta B/\sqrt{\mu_0 m_p n_p}$ which is

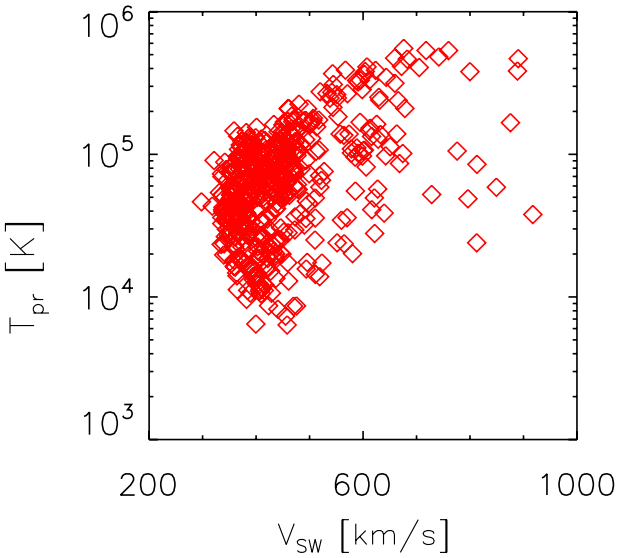

Figure 4. Scatterplot of T_{pr} as a function of V_{SW}. Winds below 500 km/s tend to be cooler than winds in the 500–800 km/s range. Winds above 800 km/s correspond to intervals of solar ejections.

the amplitude in Alfvén speed units. From this, we anticipate that ϵ evaluated with either (2) or (4) correlates with T_{pr} since ϵ depends on $\delta B/\sqrt{\mu_0 m_p n_p}$ through $P_B(\nu)/\sqrt{\mu_0 m_p n_p}$. No correlation with δB and $\delta\ B/\sqrt{\mu_0 m_p n_p}$ is found with n_p, B_0, β_p, or V_{SW}, but a correlation does exist with proton pressure $n_p k_B T_{pr}$.

6. Measurements of Predicted Cascade and Expected Rates

[41] The Kolmogorov cascade rate in (2) is evaluated using $C_K = 1.6$, $R_A = 0.5$, $\nu = 0.01$ Hz, and P_B measured at

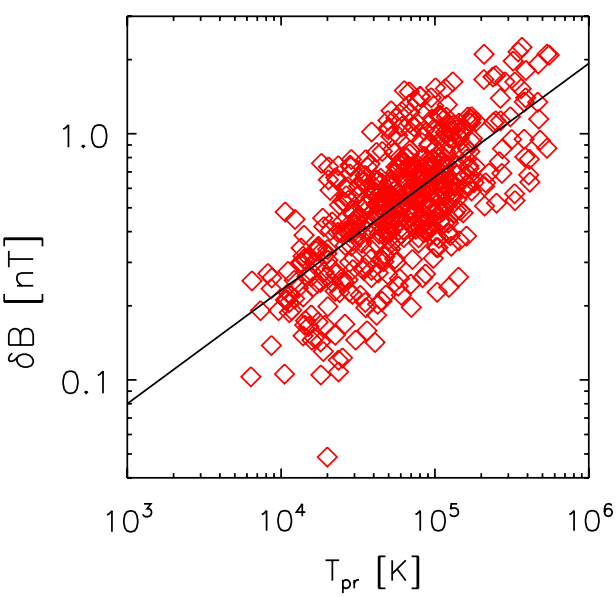

Figure 5. Scatterplot of power in integrated IMF spectrum from 0.008 to 0.1 Hz as a function of T_{pr}. Fit line parameters are given in text. The plot shows that larger amplitudes correspond to higher T_{pr}.

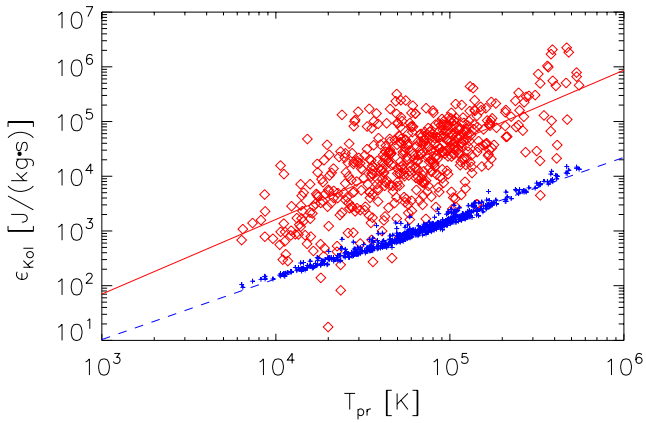

Figure 6. Scatterplot of the Kolmogorov cascade rate (red diamonds) and expected heating rate (blue crosses) as a function of T_{pr}. The Kolmogorov rate exceeds the expected one by a factor of 10 or more. Fit parameters are given in Table 3.

0.01 Hz from the fitted spectrum. Plasma parameters used in (2) are taken from averages over the intervals from which the spectrum is computed. The chosen value of $R_A = 0.5$ represents the typical value at 1 AU [e.g., *Matthaeus and Goldstein*, 1982; *Goldstein et al.*, 1995] found at lower frequencies and cannot be assessed directly at $\nu = 0.01$ Hz since velocity measurements at this frequency are not available.

[42] Figure 6 shows ϵ_{Kol} as a function of T_{pr} using diamond-shaped points and plots the least squares fit using a solid line. The expected heating rate based on (11) as a function of T_{pr} is shown with crosses, and the fit is a dashed line. Data points with T_{pr} between 10^4 and 10^5 K correspond to ϵ_{Kol} from approximately 10^3 to 4×10^4 J/(kg s), while between 10^5 and 10^6 K correspond to 4×10^4 to 10^6 J/(kg s). Observations are considerably scattered about the fit $\epsilon_{Kol} = 5.7 \times 10^{-3} T_{pr}^{1.36}$. The fit is the result of the linear least squares method used without individual uncertainties. Parameters of the fit are reported in Table 3. The relative uncertainties for ϵ_{Kol} average near 0.35 and for T_{pr} near 0.27, but these are smaller than the actual spread in the data. Thereby, there is a true distribution in ϵ_{Kol} values which is not due to uncertainties and for which the fit gives only the average trend. When fits are made using the individual measurement uncertainties, the fits are not good ones judged by the trend of the data and by very large χ^2 values. Nonlinear least squares fits have the same difficulties and do not even find a minimum when individual uncertainties are used. For all ϵ fits reported in this paper, the linear least squares method without uncertainties is employed.

[43] The expected values in Figure 6 fall tightly on a straight line. For constant V_{SW}, ϵ_{heat} is linear in T_{pr}. The data points are nonuniformly spread in V_{SW} and provide the variation around the fit line which causes the fit to vary more than linear as $\epsilon_{heat} = 4.84 \times 10^{-3} T_{pr}^{1.11}$.

[44] The expected values are a factor of 13 smaller at 10^4 K than ϵ_{Kol} and 39 smaller at 10^6 K. Because individual evaluations of the cascade rate are known to a relative accuracy of 40%, the distributions of ϵ_{Kol} and ϵ_{heat} have well separated averages which are far apart in standard devia-

Table 3. Fit Function Parameters for ϵ Versus T_{pr}

Fit Function	χ^2
$\epsilon_{heat} = (4.84^{+3.64}_{-2.07} \times 10^{-3})\ T_{pr}^{1.11\ \pm\ 0.05}$	0.03
$\epsilon_{Kol} = (5.68^{+4.27}_{-2.43} \times 10^{-3}\ T_{pr}^{1.36\ \pm\ 0.05}$	1.56
$\epsilon_{Kol,2D} = (4.21^{+3.16}_{-1.80} \times 10^{-3}) T_{pr}^{1.39\ \pm\ 0.05}$	1.47
$\epsilon_{Kr} = (5.03^{+3.78}_{-2.16} \times 10^{-6}) T_{pr}^{1.70\ \pm\ 0.05}$	2.26
$\epsilon_{Kr,2D} = (3.69^{+2.77}_{-1.58} \times 10^{-6}) T_{pr}^{1.73\ \pm\ 0.05}$	2.14

tions based on measurement error. The discrepancies remain large even if we assumed $R_A = 0$, which is unlikely, reducing the amounts by 0.54. At lower frequencies, where velocity measurements are available, our data set has an average σ_c of 0.40 ± 0.21. This indicates that $\epsilon_{Kol,c} \approx \epsilon_{Kol}$ for our data. Table 1 shows that significant reduction in $\epsilon_{Kol,c}$ only occurs for $\sigma_c > 0.95$. Moreover, for cascades where $\sigma_c \neq 0$ in the lower and middle inertial range, an analysis by *Lithwick and Goldreich* [2003] for weak turbulence determined that σ_c will approach zero in the high end and vanish at the point where the dissipation range begins [see also *Grappin et al.*, 1983], while for strong turbulence *Lithwick et al.* [2007] showed that σ_c would have the same value in the upper end as in the low end. Discrepancies are also not significantly changed by evaluating the spectral amplitude at a different frequency in the inertial range. If the spectral index is −5/3, ϵ_{Kol} has the same value at all ν in the fitted spectral band. For a spectrum with −3/2, there is more power relative to a −5/3 spectrum between the inertial and dissipation ranges which occurs at higher frequencies than 0.01 Hz. This would yield larger ϵ_{Kol} values than found at 0.01 Hz. Toward lower ν, a spectrum with −3/2 would show a reduction in ϵ_{Kol} from that at 0.01 Hz. The amount of change in either case for ϵ_{Kol} is proportional to $(\nu/0.01)^{1/4}$. This amount alone only becomes more than a factor of 10 when ν is 4 decades away from 0.01 Hz. The discrepancy is also not resolved by binning data according to spectral indices. When only data with q_{inert} between −1.62 and −1.72 are considered, no better agreement between ϵ_{Kol} and ϵ_{heat} is found.

[45] The 2-D Kolmogorov prediction (not shown) gives nearly the same distribution of values as seen for the isotropic one. Fit parameters are given in Table 3. The average value of ψ is 58° so that from (7) we find that $\epsilon_{Kol,2D} = 0.81\ \epsilon_{Kol}$. We have far too few data at small ψ to show that the two predictions differ by a statistically significant amount.

[46] Figure 7 repeats the analysis of Figure 6 but using the Kraichnan cascade rate. Equation (4) is evaluated using $A = 1.42$, $\nu = 0.01$ Hz, and P_B measured at 0.01 Hz from the fitted spectrum. Plasma parameters are again the averages during the intervals, except for V_A which is calculated using B_0 and n_p. Here the value of B_0 is the average total magnetic intensity over the interval and so includes contributions from both the background interplanetary magnetic field and fluctuations. Over all intervals, average B_0 is 7.2 nT. At the upper end of the inertial range, fluctuations are presumed to evolve in accord with the local average magnetic field as if it were the background magnetic field. If fluctuations in the higher inertial range obey the Alfvén wave dispersion relation, they then propagate at the higher speed V_A than the one associated with the interplanetary field alone. The Kraichnan cascade rate is a close match to the expected rate on average. Values for ϵ_{Kr} and ϵ_{heat} coincide near $T_{pr} = 10^5$ K where most of the data occurs but diverge at other T_{pr}. The fit function (see Table 3) has $\epsilon_{Kr} = 5.03 \times 10^{-6}\ T_{pr}^{1.70}$ which increases more steeply with T_{pr} than does ϵ_{Kol}. (The 2-D Kraichnan prediction is nearly the same as the isotropic one and fit parameters are also listed in Table 3.) The steeper fit is fairly well explained according to (5) where $\epsilon_{Kr} \propto \epsilon_{Kol}^{4/3} \propto (T_{pr}^{1.36})^{4/3} \propto T_{pr}^{1.81}$. The largest discrepancy between the Kraichnan and expected rates is found at low T_{pr}. At $T_{pr} = 10^4$, the fitted ϵ_{Kr} is smaller than ϵ_{heat} by a factor of 4.2.

[47] *Matthaeus and Zhou* [1989] developed a theory of the turbulent cascade which is a composite of the Kolmogorov and Kraichnan theories. As discussed in section 3, this gives us $A = 1.42$ when $C_K = 1.6$. The controlling parameter in the theory can be expressed as $Z_0 = (2\ \pi\nu V_A^3/(A^2\ V_{SW}\ \epsilon))^{1/3}$. We have evaluated Z_0 for our results and assumed that $\epsilon = \epsilon_{heat}$. We find that the average value of Z_0 is 27 and almost all values are above 10. This corresponds to the limit of a Kraichnan cascade in the theory of Matthaeus and Zhou and so is consistent with $\epsilon_{Kr} \approx \epsilon_{heat}$. However, their theory also predicts that the spectral index should be nearly −3/2 which is not found in Figure 3 (but see *Borovsky* [2006]).

[48] We now turn to a comparison of cascades rates as a function of solar wind speed. This approach is in accord with the determination of ϵ_{heat}. Also it serves as a different kind of ensemble averaging of the data than with T_{pr} because streams of nearly the same T_{pr} may come from both slow and fast winds and so have different origins and be associated with different governing processes near the Sun. Figure 8 shows ϵ_{heat} as a function of V_{SW}. Figure 9 shows the same for ϵ_{Kol} and Figure 10 for ϵ_{Kr}. Data points do not cover as wide a range of values as seen for T_{pr} and are mostly concentrated at speeds between 350 and 500 km/s because of nonuniform sampling with respect to V_{SW}. Table 4 gives average values and standard deviations in bins of V_{SW} with the assumption that ϵ values are log-normally distributed. This assumption is a good one and

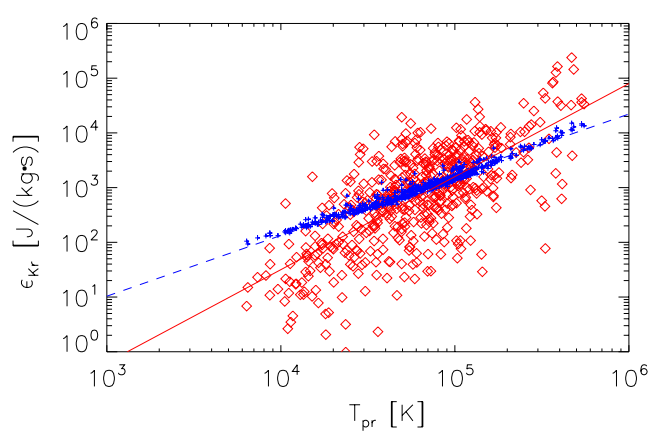

Figure 7. Scatterplot of the Kraichnan cascade rate (red diamonds) and expected heating rate (blue crosses) as a function of T_{pr}. The average Kraichnan rate is consistent with the expected rate at moderate and high T_{pr}. Fit parameters are given in Table 3.

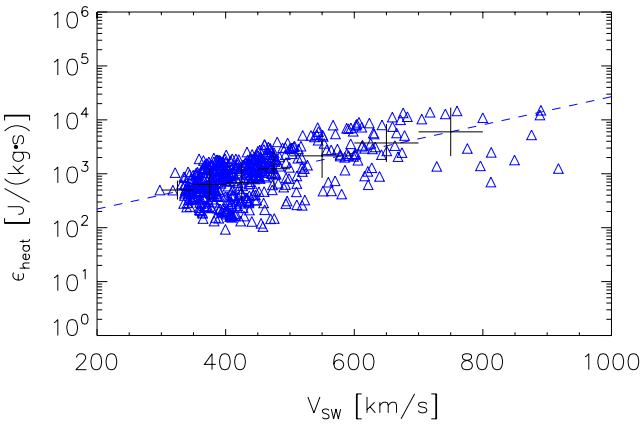

Figure 8. Scatterplot of the expected heating rate as a function of V_{SW}. Fit parameters are given in Table 5. Crosses mark bin averages and standard deviations for the heating rate per solar wind speed bins are given in Table 4.

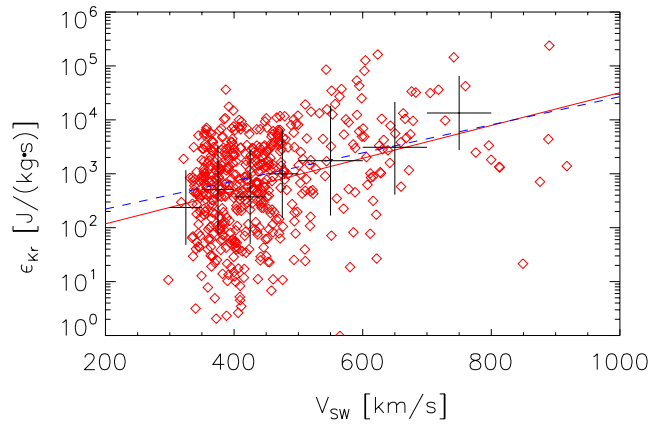

Figure 10. Scatterplot of the Kraichnan cascade rate as a function of V_{SW}. Solid line corresponds to the fit for the Kraichnan rate and the dashed line for the expected rate. Fit parameters are given in Table 5. Crosses mark bin averages and standard deviations for the Kraichnan rate per solar wind speed bins are given in Table 4. Kraichnan and expected rates are consistent with one another.

follows from the fact that magnetic field fluctuation amplitudes are themselves log-normally distributed in solar wind data and are a primary factor in the determination of ϵ_{Kol} and ϵ_{Kr}. Large crosses on Figures 8–10 show these values and ranges. Linear fits have been made to the function $\log\epsilon = a + bV_{SW}$ without regard to binning and are also shown in the figures. Solid lines in Figures 9 and 10 correspond to the fits of ϵ_{Kol} and ϵ_{Kr}, respectively, while the dashed line is the fit of ϵ_{heat}. Fit parameters are given in Table 5.

[49] Average values of ϵ_{Kol} are larger than ϵ_{heat} as a function of V_{SW} while the average values of ϵ_{Kr} are in good agreement with ϵ_{heat}. For 500 km/s, the ratio of average values is $\epsilon_{Kol}/\epsilon_{heat}$ = 19.6 and $\epsilon_{Kr}/\epsilon_{heat}$ = 0.8. The discrepancy is approximately constant as a function of V_{SW} and certainly more so than over the range of T_{pr}. Thus the data is consistent with values of C_K and A which are the same for all streams. Adjusting C_K to achieve agreement between with ϵ_{Kol} and ϵ_{heat} would require C_K = 11.6 which is even larger than the result of *Verma et al.* [1995] for Alfvénic intervals and is inconsistent with C_K being an order of unity constant. Naturally, if C_K is larger than 1.6 (even if only by a factor of 2), then following the *Matthaeus and Zhou* [1989] prescription, the value of A would become larger and Kraichnan rate would no longer agree with the expected rate. Only values of $A \approx 1.4$ are in agreement with the expected rate. The predictions from the 2-D cascade rates are nearly the same as above, and their corresponding fit parameters are given in Table 5.

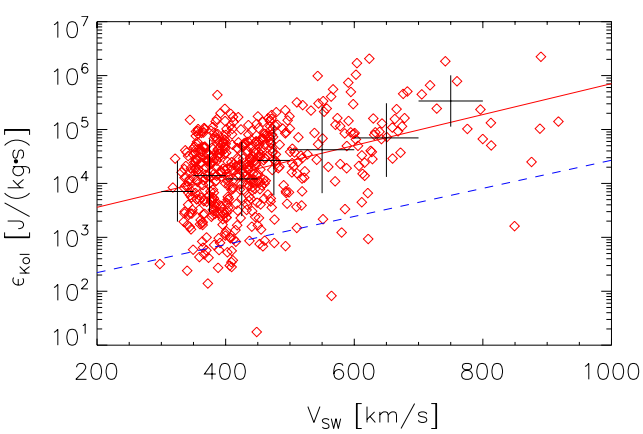

Figure 9. Scatterplot of the Kolmogorov cascade rate as a function of V_{SW}. Solid line corresponds to the fit for the Kolmogorov rate and the dashed line for the expected rate. Fit parameters are given in Table 5. Crosses mark bin averages and standard deviations for the Kolmogorov rate per solar wind speed bins are given in Table 4. The average Kolmogorov rate is a factor of 20 too large compared to what is expected.

[50] Values of the Kolmogorov rate resemble the results of *Verma et al.* [1995] concerning Alfvénic streams evaluated at much lower v and using velocity and magnetic field fluctuation data. In fact, if we rescale results in their Table 2 from $C_K = 8$ to $C_K = 1.6$ and remove the factor $\epsilon_{Kol,c}/\epsilon_{Kol}$ for $\alpha_1 = 0.07$, then we find values that are in the typical range of our data. However, at low frequencies we find that our data set corresponds to non-Alfvénic intervals. Consistency should exist with the non-Alfvénic results of Verma et al. given in their Table 1. They found four streams ranging from slow to fast which had values of ϵ_{Kol} rescaled from $C_K = 1$ to $C_K = 1.6$ which are smaller than ϵ_{heat}. In our data set this occurs only rarely. Thereby, we find that our results are not consistent with Verma et al., and we cannot explain how these differences arise.

[51] Table 4 also contains averages of V_A based only on protons and the average value of ψ. Using these average values and a value of V_{SW} at the midpoint of each bin, we list estimates of the loss differential streaming energy rate from beam-core protons using (16) with the assumption that $n_b/n_p = 0.2$, $V_{pp} = 1.1\ V_A$ for $V_{SW} < 600$ km/s and $V_{pp} = 1.25\ V_A$ for $V_{SW} > 600$ km/s based on results from *Marsch et al.* [1982]. We find that these rates range from 10–30% of the expected heating rates, except for highest V_{SW} bin where 37% is found but this bin only contains a few data points. Considering that S is probably an upper limit, we conclude that most proton heating comes from an external source. For

Table 4. Quantities Binned According to Intervals of V_{SW}, km/s[a]

Quantity	300–350	350–400	400–450	450–500	500–600	600–700	700–800
Number of data	17	170	133	86	52	34	8
$10^2\ \epsilon_{heat}$	$4.99^{+2.48}_{-1.66}$	$6.33^{+6.01}_{-3.08}$	$6.84^{+8.37}_{-3.76}$	$12.39^{+14.99}_{-6.78}$	$21.49^{+33.49}_{-13.09}$	$37.28^{+46.81}_{-20.75}$	$59.95^{+109.18}_{-38.70}$
$10^3\ \epsilon_{Kol}$	$7.02^{+19.12}_{-5.13}$	$13.93^{+51.39}_{-10.96}$	$12.11^{+51.39}_{-9.63}$	$26.67^{+92.37}_{-20.69}$	$42.18^{+227.55}_{-35.59}$	$69.84^{+237.40}_{-56.63}$	$337.82^{+673.18}_{-224.94}$
$10^3\ \epsilon_{Kol,2D}$	$6.93^{+18.88}_{-4.49}$	$13.78^{+50.22}_{-10.91}$	$12.25^{+46.56}_{-9.70}$	$27.62^{+91.76}_{-21.23}$	$45.35^{+250.52}_{-38.40}$	$72.60^{+254.71}_{-56.49}$	$300.38^{+723.10}_{-212.22}$
$10^2\ \epsilon_{Kr}$	$2.37^{+9.29}_{-1.89}$	$5.09^{+28.51}_{-4.32}$	$3.72^{+24.08}_{-3.22}$	$9.96^{+55.58}_{-8.45}$	$17.46^{+163.84}_{-15.78}$	$31.01^{+184.24}_{-26.54}$	$133.93^{+518.39}_{-106.43}$
$10^2\ \epsilon_{Kr,2D}$	$2.32^{+9.18}_{-1.85}$	$4.99^{+27.35}_{-4.22}$	$3.72^{+23.61}_{-3.21}$	$10.21^{+55.52}_{-8.63}$	$18.57^{+178.25}_{-16.82}$	$31.90^{+172.55}_{-26.92}$	$117.85^{+537.10}_{-96.64}$
$\epsilon_{Kol}/\epsilon_{heat}$	14.06	21.98	17.71	21.54	19.63	18.74	56.35
$\epsilon_{Kol,2D}/\epsilon_{heat}$	13.89	21.75	17.91	22.31	21.10	19.48	50.11
$\epsilon_{Kr}/\epsilon_{heat}$	0.47	0.80	0.54	0.80	0.81	0.83	2.23
$\epsilon_{Kr,2D}/\epsilon_{heat}$	0.46	0.79	0.54	0.82	0.86	0.86	1.97
V_A	42	51	62	65	67	77	175
ψ	58°	59°	59°	57°	55°	56°	69°
S	70	111	195	255	348	647	2242
ξ_{avg}	0.72	0.73	0.74	0.75	0.81	0.85	0.78

[a]Values of ϵ are averaged in log space. V_A is the average Alfvén speed in km/s based only on protons. S is the streaming energy loss rate from (16) in units of J/(kg s).

$V_{SW} < 600$ km/s, average ϵ_{Kr} is less than ϵ_{heat} by as much as 50% and so some additional source such as from differential streaming could be needed. However, we need to consider further the uncertainty in determining values of ϵ_{heat}.

[52] The equation of state for the protons is a source of uncertainty because we have neglected terms even in the radially symmetric limit as discussed in section 3. Moreover, T_{pr} does not correspond to the total thermal energy of protons as would T_p and so the complete energization of the protons is not definitively known. We have estimated the uncertainty from these by using typical values for solar wind parameters at 1 AU (see Appendix B for details) and evaluating the more complete equation of state in (13). As discussed in section 3, we expect average T_{pr} to be nearly the same as T_p when average ψ is near 54.74°. There is an important difference between the index ξ_{avg} characterizing T_p change with r and ξ characterizing T_{pr}. For the case $\xi = 0.9$, we have found values of ξ_{avg} listed in Table 4 with an average near 0.75. This causes ϵ_{heat} to be underestimated by using (11). On average we find that ϵ_{heat} should be 1.22 times greater than its value calculated from (11). This would increase the discrepancy between ϵ_{Kr} with ϵ_{heat}. More can be said about these uncertainties in terms of an energy diagram to which we now turn.

[53] For our final analysis of the data, we consider rates as a function which is proportional to the product of $V_{SW}\ T_{pr}$. This will have values of the expected heating rate following a straight line from which the significance of the results can be summarized and quantified. Figure 11 plots cascade and expected heating rates as a function of ϵ_{heat} which is defined in (11) and corresponds to the case where $\xi = 0.9$. Dashed lines give the expected heating rate ϵ for different values of ξ where $\epsilon = (4/3 - \xi)\ \epsilon_{heat}/(4/3 - 0.9)$ (see equation (10)). In this log-log plot these expected rates follow straight lines with slope 1 and are labeled with the value of ξ where numbers in parenthesis correspond to negative values. The thicker black dashed line corresponds to zero temperature gradient ($\xi = 0$) and divides an upper region where T_{pr} rises with increasing distance from a lower one where T_{pr} falls. The thick solid lines correspond to fits of the trend for the Kolmogorov and Kraichnan predictions. Fit parameters are given in Table 6. These lines have slopes greater than 1 with the Kraichnan rate having larger slope. Since T_{pr} has a far greater range of values than V_{SW}, these trend lines are similar to what is found when the cascade rates are plotted as a function of only T_{pr}.

[54] The trend line for ϵ_{Kol} in the plotted range is located entirely in the upper region. In situ heating at 1 AU would then be greater than adiabatic cooling. The value of T_{pr} would be expected to increase with increasing r with $\xi \approx -8$. Clearly, this prediction is out of bounds with respect to protons which cool in net with increasing r. For the case $\xi = 0.9$, uncertainty associated with the equation of state about the average value of ϵ is shown in the figure by the vertically hatched fill lines. The primary source of uncertainty in (13) is due to plasma anisotropy rather than change of speed with r or heat flux. If the true values of T_p and ξ_{avg} were known, the relative uncertainty in using an expression like (11) would be 30%. However, in using T_{pr} and ξ, the total relative uncertainty is about 50% and has average values about 22% higher than the line $\xi = 0.9$ because the average value of ξ_{avg} is smaller than ξ. Uncertainty in temperature from evaluating ϵ_{heat} from (11) simply moves one along the line of slope 1. Thereby, the uncertainty here is confined to the strip shown.

[55] The average value of ϵ_{Kol} is far larger than expected for proton heating and cannot be explained by uncertainties in the analysis. If protons cannot take up the excess cascade energy in the Kolmogorov prediction, then the excess would need to heat other plasma species. However, in section 3, we have argued that alphas and electrons are heated by a lesser amount than protons from the turbulent cascade. Certainly, a factor of more than 10 excess flowing to other

Table 5. Fit Function Parameters for ϵ Versus V_{SW}, km/s

Fit Function	χ^2
$\ln \epsilon_{heat} = 4.20 \pm 0.2 + (0.0060 \pm 0.0004)\ V_{SW}$	0.60
$\ln \epsilon_{Kol} = 6.87 \pm 0.2 + (0.0066 \pm 0.0004)\ V_{SW}$	2.52
$\ln \epsilon_{Kol,2D} = 6.90 \pm 0.2 + (0.0066 \pm 0.0004)\ V_{SW}$	2.49
$\ln \epsilon_{Kr} = 3.37 \pm 0.2 + (0.0070 \pm 0.0004)\ V_{SW}$	3.93
$\ln \epsilon_{Kr,2D} = 3.38 \pm 0.2 + (0.0070 \pm 0.0004)\ V_{SW}$	3.90

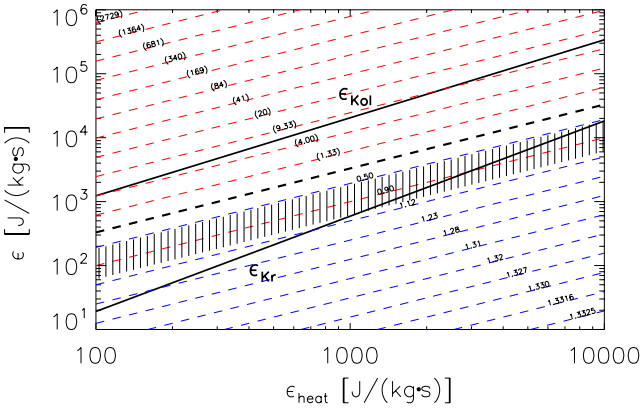

Figure 11. Energy cascade rate diagram plots ϵ as a function of ϵ_{heat}. Dashed lines marked with ξ give the expected heating rate for that temperature gradient. Values enclosed in parenthesis are negative. The lined pattern fill about line of $\xi = 0.9$ is the uncertainty range based on the equation of state. The bold dashed line corresponds to $\xi = 0$ dividing an increasing T_{pr} wind in the upper portion of the diagram from a decreasing one below. Dashed line spacing is a factor of 2 except between the line for $\xi = 0.5$, which is included by preference. The solid line in the upper portion of the diagram is the Kolmogorov rate and lower solid line is the Kraichnan rate. Fit parameters are given in Table 6.

species has not been reported. Moreover, since we expect that most proton heating is due to external sources, cascade rates in the high end of the inertial range should be comparable to ones estimated in the energy containing scales. These energy-containing scale rates are in agreement with values of ϵ_{heat} [*Smith et al.*, 2001a, 2006c; *Isenberg*, 2005]. That these do not match what is found using (2) shows that ϵ_{Kol} does not properly evaluate the cascade rate for solar wind turbulence at 1 AU in the high end of the inertial range.

[56] The Kraichnan cascade rate does come into the expected range of agreement when $\epsilon_{heat} > 1000$ J/(kg s). In the plotted range, the Kraichnan prediction is within the lower portion of the plot where T_{pr} falls with increasing r. Thus the prediction gives average values which are at least possible for a mainly proton heated solar wind. Below $\epsilon_{heat} =$ 1000 J/(kg s), the prediction departs below ϵ_{heat} with $\xi =$ 0.9. As a function of V_{SW}, ϵ_{Kr} was in agreement with ϵ_{heat} with $\xi = 0.9$ which is essential because this is how the average value of ξ was found. However, in this plot, T_{pr} plays a large role, and we do not know if the average value of ξ is a function of T_{pr}. If the Kraichnan prediction is a good estimate of the cascade rate, then its trend line forecasts that at lower values of ϵ_{heat}, and so also of T_{pr} (see Figure 7), that the solar wind heating rate should correspond to ones with ξ closer to the adiabatic value of 4/3. We are not aware of a published complete study of ξ as a function of T_{pr} from which to verify this forecast. We thereby conclude that our results cannot discount the Kraichnan prediction as a method to evaluate turbulent cascade rates.

[57] Qualitatively, a good case can be made for a dependence of ξ on T_{pr}. First, Figure 5 shows that wave amplitudes increase with increasing T_{pr} spanning a temperature range of nearly 100. The proton temperature in the corona is likely confined to a smaller range near $1-3 \times 10^6$ K. The large spread in T_{pr} found at 1 AU could result from the accumulative effects of turbulent heating wherein strongly heated solar wind with larger amplitude fluctuations results in a higher temperature at 1 AU and so a smaller net change of temperature from the corona. If true, then the temperature gradient would depend on the energization of protons from the turbulent energy cascade and show a dependence on T_{pr}. Second, the dependence of ξ on T_{pr} could account for why average ϵ_{heat} per solar wind bins below 600 km/s are greater than ϵ_{Kr}. There is a distinct asymmetry below the fit line in Figure 10, where ϵ_{Kr} has values even below 20 J/(kg s). This asymmetry is not so pronounced for ϵ_{heat} in Figure 8 and this could be due to using $\xi = 0.9$ for all data points. If ξ does become larger with decreasing T_{pr}, this would increase the spread below the shown fit line and most probably lower the mean value of ϵ_{heat} into better agreement with ϵ_{Kr}. Finally, some evidence for a temperature trend consistent with the Kraichnan prediction can be found in the work of *Freeman and Lopez* [1985]. They reported that around solar maximum 3–10% of the solar wind intervals are characterized by an expectational low T_{pr} defined as values below 15,000 K. They concluded that these intervals are consistent with almost adiabatic expansion because with this assumption T_{pr} at the Sun would match observed coronal temperatures.

7. Prediction of the Cascade Rate as a Function of Heliocentric Distance

[58] The discrepancies for the Kolmogorov rate continue to be problematic when we consider the probable behavior of the cascade rate with heliocentric distance r. The dependence of ϵ_{Kol} with r can be determined by knowing the dependence of P_B, n_p, and V_{SW} where ν is treated as a constant. The value of P_B depends on the square of the magnetic field fluctuation amplitude. This amplitude is observed [e.g., *Roberts et al.*, 1990] to follow closely the geometrical optics prediction [e.g., *Völk and Alpers*, 1973] of $r^{-1.5}$ for $r > 0.3$ AU so that P_B obeys r^{-3}. In a spherically expanding solar wind, density varies as r^{-2}. The solar wind speed can be taken to be a constant with reasonable accuracy. The value of ϵ_{Kol} can then be shown to vary as $r^{-1.5}$ and has this functional form both inside and outside of 1 AU. From (9) and using $\xi = 0.9$, ϵ_{heat} varies $r^{-1.9}$. Then, $\epsilon_{Kol}/\epsilon_{heat}$ varies as $r^{0.4}$. Inside of 1 AU, ϵ_{Kol} on average (i.e., using values from our derived fit function) will approach ϵ_{heat} with decreasing r. Outside of 1 AU, ϵ_{Kol} will diverge from ϵ_{heat} with increasing r.

[59] A perpendicular cascade is what is actually expected to occur in the solar wind. At 1 AU, we find no distinction

Table 6. Fit Function Parameters for ϵ Versus ϵ_{heat}

Fit Function	χ^2
$\epsilon_{Kol} = (4.48^{+1.63}_{-1.19})\ \epsilon_{heat}^{1.22\ \pm\ 0.05}$	1.55
$\epsilon_{Kol,2D} = (3.42^{+1.24}_{-0.91})\ \epsilon_{heat}^{1.24\ \pm\ 0.05}$	1.46
$\epsilon_{Kr} = (0.02^{+1.34\ \times\ 10^{-2}}_{-2.0\ \times\ 10^{-3}})\ \epsilon_{heat}^{1.49\ \pm\ 0.05}$	2.31
$\epsilon_{Kr,2D} = (0.02^{+5.7\ \times\ 10^{-3}}_{-6.2\ \times\ 10^{-3}})\ \epsilon_{heat}^{1.51\ \pm\ 0.05}$	2.21

between the isotropic and 2-D cases. In this case, we continue to associate the perpendicular fluctuations with ones which maintain a constant frequency with distance. This is not the only possibility since expansion can enlarge perpendicular scales with increasing r, but the complete role of expansion is not yet known (M. Velli, private communication, 2006). Outside of 1 AU, ϵ_{Kol} and $\epsilon_{Kol,\,2D}$ will remain nearly the same since the interplanetary magnetic field tends toward the azimuthal direction. The discrepancy inside of 1 AU is actually increased by using $\epsilon_{Kol,2D}$ as compared to ϵ_{Kol}, and spacecraft data inside of 1 AU should be able to distinguish the two cases. Inside of 1 AU, the interplanetary magnetic field approaches the radial direction with decreasing r. For a Parker interplanetary magnetic field, sin ψ varies nearly as r inside of 1 AU. The factor 1/sin ψ in $\epsilon_{Kol,2D}$ would then result in a $r^{-2.5}$ functional dependence. The value of $\epsilon_{Kol,2D}/\epsilon_{heat}$ then varies as $r^{-0.6}$ which increases the discrepancy found at 1 AU by a factor of 2 at 0.3 AU.

[60] The Kraichnan rate at 1 AU is in closer agreement with the expected heating rate. Inside of 1 AU, ϵ_{Kr} varies as r^{-1} assuming constant V_{SW}, and outside of 1 AU, where V_A is nearly constant, ϵ_{Kr} varies as r^{-2}. Inside of 1 AU, $\epsilon_{Kr}/\epsilon_{heat}$ varies as $r^{0.9}$ and on average this ratio will decrease with decreasing r. At 0.3 AU, this would bring most values of ϵ_{Kr} to values that are one-third of ϵ_{heat}. Outside of 1 AU, $\epsilon_{Kr}/\epsilon_{heat}$ varies $r^{-0.1}$ and so this ratio will only slowly decrease with increasing r. For most values of T_{pr}, ϵ_{Kr}, and ϵ_{heat} will remain close out to 10 AU. *Verma et al.* [1995] noted that heating rates could not be consistently matched inside and outside of 1 AU and so concluded that the isotropic Kraichnan prediction was not valid. However, this situation might be remedied by the 2-D Kraichnan prediction. Outside of 1 AU, ϵ_{Kr} and $\epsilon_{Kr,2D}$ will remain nearly the same since, as before, the interplanetary magnetic field tends toward the azimuthal direction. Inside of 1 AU, the factor 1/sin ψ within $\epsilon_{Kr,2D}$ nearly compensates for the decrease of $\epsilon_{Kr}/\epsilon_{heat}$ with decreasing r so as to keep $\epsilon_{Kr,2D}$ close to ϵ_{heat}. In fact, $\epsilon_{Kr,2D}/\epsilon_{heat}$ varies as $r^{-0.1}$ inside of 1 AU.

8. Summary and Conclusions

[61] We have used 526 measured magnetic field fluctuation power spectra from the high end of the inertial range to evaluate cascade rates based on Kolmogorov and Kraichnan predictions. The cases span a 4 year period about the peak of solar activity in 2000. Measurements mostly correspond to slow wind but there is an extensive range of proton temperature. Spectral indices average near $-5/3$ but show no tendency to narrow in range at large proton temperatures. Integrated magnetic field fluctuation amplitudes in the high end of the inertial tend to increase with increasing temperature. Since amplitude is the primary factor in the evaluation of cascade rates, both Kolmogorov and Kraichnan rates also increase with temperature.

[62] The cascade rates have been compared to expected ones based on proton heating. Evaluation of uncertainties from the equation of state indicate that on average an estimate within a factor of 2 is obtained using the available radial component of the proton temperature. Furthermore, we expect that protons are heated more by the turbulent energy cascade than are alphas and electrons. The Kolmogorov prediction (2) with $C_K \approx 1.6$ (the value determined in hydrodynamic experiments) is found to be a factor of 10 or more above the expected rate (11), while the Kraichnan prediction (4) with $A \approx 1.4$ (the value given in the *Matthaeus and Zhou* [1989] model) is consistent with the expected rate. On average, the Kolmogorov rate is a factor of 20 greater than expected. If this discrepancy entirely rests with C_K, then $C_K \approx 12$ is required to resolve the difference, but then C_K is not a constant of order unity as expected. With large C_K, the estimated interaction time between turbulent eddies in the Kolmogorov model for solar wind magnetic field fluctuations is far longer than the nonlinear turnover time which governs hydrodynamic eddies. This might indicate that the nonlinear turnover time does not alone govern the interactions at the high end of the inertial range for the solar wind case. On the other hand, the Kraichnan model with A of order unity can potentially account for the longer interaction times with the wave effects included in this model. No distinction between isotropic and 2-D forms is found in the data, but this is to be expected because in most of our cases the magnetic field is not near the radial direction. However, consideration of the behavior of the predictions with heliocentric distance, finds that the 2-D Kraichnan rate best follows the expected trend of the proton heating rate with heliocentric distance. We conclude that the 2-D Kraichnan prediction is the best available estimator of the cascade rate for use in the high end of the inertial range.

Appendix A: Reduced Spectra and the 2-D Cascade Rate

[63] The predictions of Kolmogorov and Kraichnan cascades employ the omnidirectional value of the spectral power density. The measured spectrum P_B is the reduced spectrum observed along one line of sight. The relation between the two is needed to give an expression that can be evaluated from measurements. In the isotropic case, the omnidirectional spectrum is $4\pi A_0 k^2 k^{q-2}$ where k is the total wave number and q is the spectral index. The factor of 4π represents the total contribution of the power in that wave number across the entire sphere. The value of A_0 is the scaling parameter in the energy spectrum $A_0\ k^{q-2}$. If we pick a particular axis, say the $\pm x$ direction, and integrate $A_0\, k^{q-2}$ over all wave numbers transverse to the $\pm x$ direction, one finds that the isotropic case leads to an integral of this form by trigonometric substitution:

$$P_B = 4\pi A_0 k_x^q \int_0^{\pi/2} \sin\phi \cos^{-q-1}\phi\, d\phi, \qquad \text{(A1)}$$

where $\tan\phi = \sqrt{k_y^2 + k_z^2}/k_x$. The integral can be related to a beta function B(m, n) and gamma functions with the relation

$$\int_0^{\pi/2} \sin^{2m-1}\phi \cos^{2n-1}\phi d\phi = \frac{1}{2}B(m,n) = \frac{\Gamma(m)\Gamma(n)}{2\Gamma(m+n)}. \qquad \text{(A2)}$$

For the isotropic case, $m = 1$ and $n = -q/2$, and combined with the recursion relation $\Gamma(1 + n) = n\Gamma(n)$, one can show

that the integral reduces simply to $-1/q$. The needed relation between the reduced and the omnidirectional value is then $-qP_B(k) = 4\pi A_0\, k^q$. This explains why the absolute value of the applicable spectral index is seen in (2) and (4) in association with P_B.

[64] The 2-D case requires a new calculation of the reduced and omnidirectional spectrums. Here, the omnidirectional spectrum is $2\pi k k^{q-1}$ where power is averaged over the 2π circle about the background magnetic field direction. Let x be in the direction of the magnetic field and the yz plane contain the wave vectors of the fluctuations. First, reduce the spectrum $A_0 k^{q-1}$ to the one for the $\pm y$ direction by integrating over all k_z which leads to the following integral expression

$$P_B = \left(2\pi A_0 k_y^q\right)\left(\frac{2}{\pi}\right)\int_0^{\pi/2} \cos^{-q-1}\phi\, d\phi. \tag{A3}$$

The integral can be further expressed as

$$P_B = \left(2\pi A_0 k_y^q\right)\left(\frac{2}{\pi}\right)\frac{\sqrt{\pi}\,\Gamma(-q/2)}{2\Gamma(1/2-q/2)}. \tag{A4}$$

Equation (A4) does not reduce to a rational fraction, and so we have evaluated the integrals numerically for the Kolmogorov case $\int_0^{\pi/2}\cos^{2/3}\phi d\phi = 1.120251$ and the Kraichnan case $\int_0^{\pi/2}\cos^{1/2}\phi\, d\phi = 1.198140$. From here, the relation between the reduced and omnidirectional spectra in wave number follows.

[65] Since the direction of measurement in the solar wind will be in the radial direction, let the y direction be in the plane rx. Then it can be shown that $k_r = k_y\,|\sin\psi|$ and let $k_r = 2\,\pi\nu/V_{SW}$. The scaling factor $A_0 \equiv \delta B^2 k_0^{-q+1}$ must also be converted from wave number to ν. With all of this, the 2-D Kolmogorov prediction can then be given as

$$\epsilon_{Kol,2D} = (2\pi/V_{SW})\left|\sin^{-1}\psi\right|\nu^{5/2} \cdot \left[(1+R_A)(1.402182)\left(P_B(\nu)/\mu_0 m_p n_p\right)/C_K\right]^{3/2} \quad \text{(A5)},$$

and the 2-D Kraichnan as

$$\epsilon_{Kr,2D} = (2\pi/V_{SW})\left|\sin^{-1}\psi\right|V_A^{-1}\nu^3 \cdot \left[(1.311029)\left(P_B(\nu)/\mu_0 m_p n_p\right)/A\right]^2. \tag{A6}$$

Appendix B: Method Used to Evaluate the Equation of State

[66] We do not have all the measurements needed to evaluate the more complete equation of state in (13). However, we can use the known statistical properties of the missing solar wind values at 1 AU to evaluate ϵ from (13) and then compare with (11). On this basis, we can assess how well ϵ_{heat} is known when we neglect terms in (13).

[67] We draw from average values of measurements and then use a Gaussian function $G(\mu, >\sigma, <\sigma)$ to distribute these values about the most probable value μ, where different standard deviations σ are used above μ, denoted by $>\sigma$, and below by $<\sigma$. Table B1 summarizes the assignments. We use an ensemble of 10,000 evaluations per data point from our 526 cases to find average values of ϵ and standard deviations. Results differ little from using 1000 evaluations per data point, and so we believe that the results are statistically accurate.

[68] The measurements which we have for all 526 cases are the average magnetic field intensity B_0, the angle ψ_0 between the background magnetic field and the radial direction which here we restrict to the range 0 and 90°, the total proton density n_p, the radial component of the proton bulk speed V_{SW}, and the radial component of proton temperature T_{pr}. To evaluate (13), the quantities that we need to represent in a statistical fashion are the total proton anisotropy $\mathcal{A}$ and parallel heat flux, relative concentration and differential speed of the proton beam, alpha number density, for which we have measurements in 500 cases, and the change with heliocentric distance r of the background magnetic field, $\mathcal{A}$, parallel heat flux, and proton differential speed. Below, we discuss the assignment of values.

[69] We will assume a radial symmetric background magnetic field $\mathbf{B}_0$ in the $r\phi$ plane. This field has components $B_r = B_0\cos\psi_0\,(r_0/r)^2$ and $B_\phi = -B_0\sin\psi_0\,(r_0/r)$ where B_0 and ψ_0 are the measured values at r_0, corresponding to 1 AU. The form of B_r satisfies a divergence-free field in the radial limit. The form of B_ϕ corresponds to a current-free field, and its $1/r$ behavior is reasonably in accord with the average behavior of B_ϕ near 1 AU. Changes in field intensity and ψ will be needed in the equation of state. The change in field intensity $\partial B/\partial r$ can be shown to be

$$\frac{1}{B}\frac{\partial B}{\partial r} = -\frac{2\cos^2\psi_0 r_0^4/r^5 + \sin^2\psi_0 r_0^2/r^3}{\cos^2\psi_0 r_0^4/r^4 + \sin^2\psi_0 r_0^2/r^2}. \tag{B1}$$

When (B1) is evaluated at r_0, we find that $(1/B)\,(\partial B/\partial r) = -(2\cos^2\psi_0 + \sin^2\psi_0)/r_0$. The change of ψ with r can be derived by differentiating the ratio $-B_\phi/B_r$ which can be rewritten as $\tan\psi = \tan\psi_0(r/r_0)$. From this we find that $\partial\psi/\partial r$ is

$$\frac{\partial\psi}{\partial r} = \frac{\sin\psi_0\cos^2\psi}{r_0\cos\psi_0}, \tag{B2}$$

which at r_0 is $(\sin\psi_0\cos\psi_0)/r_0$.

[70] The protons will be taken to be a combination of a core and beam with known total density n_p. The relative beam concentration n_b/n_p at 1 AU is near 0.2 according to *Marsch et al.* [1982, Figure 16] and we assign using $G(0.2, >0.15, <0.05)$. We neglect any change in n_b/n_p with r. Core protons will be assumed to move at the speed V_{SW} in the radial direction. The proton beam will also move at this speed with the addition of a component of velocity $\mathbf{V}_{pp}$ along the known $\mathbf{B}_0$. Then, the total proton velocity components are $U_{pr} = V_{SW} + (n_b/n_p)\,V_{pp}\cos\psi$ and $U_{p\phi} = -(n_b/n_p)\,V_{pp}\sin\psi$. The change in r of the proton bulk velocity components can be written as

$$\frac{\partial U_{pr}}{\partial r} = \frac{\partial V_{SW}}{\partial r} + \frac{n_b}{n_p}\left(\cos\psi\frac{\partial V_{pp}}{\partial r} - V_{pp}\sin\psi\frac{\partial\psi}{\partial r}\right), \tag{B3}$$

$$\frac{\partial U_{p\phi}}{\partial r} = -\frac{n_b}{n_p}\left(\sin\psi\frac{\partial V_{pp}}{\partial r} + V_{pp}\cos\psi\frac{\partial\psi}{\partial r}\right). \tag{B4}$$

Table B1. Statistical Assignment of Solar Wind Quantities

Quantity	V_{SW} Range, km/s	Functional Form
n_b/n_p	all	$G(0.2, >0.15, <0.05)$
γ_{acc}	$V_{SW} < 319$	$G(0.135, 0.038, 0.038)$
	$319 \le V_{SW} < 354$	$G(0.062, 0.032, 0.032)$
	$354 \le V_{SW} < 391$	$G(0.016, 0.037, 0.037)$
	$391 \le V_{SW} < 447.5$	$G(-0.021, 0.041, 0.041)$
	$V_{SW} \ge 447.5$	$G(-0.010, 0.038, 0.038)$
V_{pp}/V_A	$V_{SW} < 400$	$G(1.1, >0.3, <0.2)$
	$400 \le V_{SW} < 600$	$G(1.1, >0.4, <0.2)$
	$V_{SW} \ge 600$	$G(1.25, >0.5, <0.1)$
n_α/n_p	all	$G(0.03, >0.01, <0.01)$
dV_{pp}/dr	all	$G(-(0.1 + \cos^2 \psi_0)$ $V_{pp}/r_0, >0.5, < 0.5)$
$\mathcal{A}$	$V_{SW} < 500$	$G(0.6, 0.2, 0.15)$
	$500 \le V_{SW} < 600$	$G(0.7, 0.3, 0.15)$
	$V_{SW} \ge 600$	$G(0.8, 0.3, 0.15)$
$d\mathcal{A}/dr$	all	$G(-0.5\mathcal{A}/r_0, >0.5, < 0.5)$
$q_\parallel$	all	$G(0.1\ q_{\parallel,0}, <0.5, >0.5)$
$dq_\parallel/dr$	all	$G(0.1\ d\ q_{\parallel,0}/dr, >0.5, <0.5)$

We first consider the change for V_{SW} with r and then for differential speed.

[71] The change of V_{SW} with r can be found in the work of *Arya and Freeman* [1991] based on power law fits where $V_{SW} = V_{SW,0}\ (r/r_0)^{\gamma_{acc}}$. We take values in their Table 3 for solar maximum and assign as given in Table B1.

[72] Differential streaming speed V_{pp} will be assigned with respect to the local value of V_A based on *Marsch et al.* [1982, Figure 13] and is given in Table B1. To evaluate V_A, we use both proton and alpha number densities and masses and neglect the small mass of electrons. In 500 cases the alpha density is known. For the remaining 26 cases, relative alpha concentration is assigned with $G(0.03, >0.01, <0.01)$ based on our data. The change of V_{pp} with r is taken to follow approximately V_A and is assigned with $G(-(0.1 + \cos^2 \psi_0)\ V_{pp}/r_0, >0.5, < 0.5)$, where r_0 is 1 AU in units of kilometers. Actually, the term proportional to $\cos^2 \psi_0$ is the change of V_A with r assuming a constant solar wind speed. The standard deviation here is assigned to get a wide spread of values. In all cases here, we do not have detailed estimates of speed gradients to draw from and so assign values as shown. When this form of differential streaming is substituted into (B4), one will find on average that $U_{p\phi}$ is approximately constant with r. In a cold solar wind without forces decelerating the beam, $U_{p\phi}$ would vary as $1/r$, and nearly so even in a warm solar wind.

[73] Proton total temperature anisotropy $\mathcal{A}$ and its change with r are taken from *Marsch et al.* [1982, Figure 15]. The assignment of $\mathcal{A}$ is given in Table B1. The average proton temperature T_p can then be found using (15) with the known radial proton temperature T_{pr}. Results discussed in the text are obtained by assuming that the gradient of T_{pr} has a power law index $\xi = 0.9$. Taking the derivative of r in (15) relates the gradients of T_p and T_{pr} by

$$\frac{\partial T_p}{\partial r} = \frac{1+2\mathcal{A}}{3}\frac{1}{\cos^2\psi + \mathcal{A}\sin^2\psi}\frac{\partial T_{pr}}{\partial r} + \frac{T_{pr}(1+2\mathcal{A})}{3\left(\cos^2\psi + \mathcal{A}\sin^2\psi\right)}\left[\frac{2}{1+2\mathcal{A}} - \frac{\sin^2\psi}{\cos^2\psi + \mathcal{A}\sin^2\psi}\right]\frac{\partial \mathcal{A}}{\partial r} - 2T_{pr}\frac{(1+2\mathcal{A})}{3}\frac{(\mathcal{A}-1)\sin\psi\cos\psi}{\left(\cos^2\psi + \mathcal{A}\sin^2\psi\right)^2}\frac{\partial\psi}{\partial r}. \quad \text{(B5)}$$

The change of $\mathcal{A}$ with r is assigned as $G(-0.5\ \mathcal{A}/r_0, > 0.5, <0.5)$ where $r_0 = 1.5 \times 10^{11}$ m or 1 AU. We take $T_p = T_{p0}\ (r_0/r)^{\xi_{avg}}$ and can determine ξ_{avg} at r_0 as

$$\xi_{avg} = \xi - r_0\left[\frac{2}{1+2\mathcal{A}} - \frac{\sin^2\psi_0}{\cos^2\psi_0 + \mathcal{A}\sin^2\psi_0}\right]\frac{\partial\mathcal{A}}{\partial r} + \frac{2(\mathcal{A}-1)}{\cos^2\psi_0 + \mathcal{A}\sin^2\psi_0}\sin^2\psi_0\cos^2\psi_0. \quad \text{(B6)}$$

In our evaluations, we find that the term dependent on the change of anisotropy with r has only a small effect and that most of the difference from ξ is due to the change of ψ_0 with r.

[74] *Feldman et al.* [1973] showed that the average value of the parallel heat flux $q_\parallel$ is $0.1q_{\parallel,0}$ where $q_{\parallel,0} = 1.5\ n_p m_p\ (k_B T_p/m_p)^{3/2}\ (3/(1 + 2\ \mathcal{A}))^{1/2}$. They also found an additional term which depends on $\mathcal{A}$, but *Marsch et al.* [1982] reported that this dependence was not seen in their data. Instead, $q_\parallel$ has a wide spread about $q_{\parallel,0}$. Therefore we assign $q_\parallel$ according to $G(0.1q_{\parallel,0}, <0.5, >0.5)$ where the standard deviation is a guesstimate. The change of $q_\parallel$ with r is computed from the definition of $q_{\parallel,0}$ and is then assigned with $G(0.1dq_{\parallel,0}/dr, >0.5, <0.5)$.

[75] **Acknowledgments.** The authors thank the ACE/SWEPAM team for providing the thermal proton data used in this study. CWS, KH, and BTM are funded by Caltech subcontract 44A-1062037 to the University of New Hampshire in support of the ACE/MAG instrument. BJV is supported by the NASA SR and T program under grant NNG06GB36G and the Living with a Star program under grant NNG05GD32G and NNX06AB85G to the University of New Hampshire. Work by BJV was done in collaboration with the Living with a Star focus team on heliospheric magnetic fields. The authors gratefully acknowledge helpful conversations with A. Bhattacharjee, B. Chandran, J. Dorelli, C. Farrugia, M. Forman, J. Hollweg, P. Isenberg, S. Markovskii, C.-S. Ng, and M. Velli. The authors also thank the referees for their helpful comments.

[76] Steven R. Cranmer thanks the reviewers for their assistance in evaluating this paper.

References

Arya, S., and J. W. Freeman (1991), Estimates of solar wind velocity gradients between 0.3 and 1 AU based on velocity probability distributions from Helios 1 at perihelion and aphelion, *J. Geophys. Res.*, *96*, 14,183.

Barakat, A. R., and R. W. Schunk (1982), Transport equations for multicomponent anisotropic space plasmas: A review, *Plasma Phys.*, *24*, 389.

Beresnyak, A., and A. Lazarian (2006), Polarization intermittency and its influence on MHD turbulence, *Astrophys. J.*, *640*, L175.

Bhattacharjee, A., and C. S. Ng (2001), Random scattering and anisotropic turbulence of shear Alfvén wave packets, *Astrophys. J.*, *548*, 318.

Bhattacharjee, A., C. W. Smith, and B. J. Vasquez (2006), Interplanetary anisotropic fluctuation spectra: Testing weakly compressible MHD theory with ACE data, *AAS Bull.*, *38*(2), 244.

Biskamp, D., and W.-C. Müller (2000), Scaling properties of three-dimensional isotropic magnetohydrodynamic turbulence, *Phys. Plasmas*, *7*, 4889.

Biskamp, D., and E. Schwarz (2001), On two-dimensional magnetohydrodynamic turbulence, *Phys. Plasmas*, *8*, 3282.

Biskamp, D., and H. Welter (1989), Dynamics of decaying two-dimensional magnetohydrodynamic turbulence, *Phys. Fluids*, *1*, 1964.

Boldyrev, S. (2005), On the spectrum of magnetohydrodynamic turbulence, *Astrophys. J.*, *626*, L37.

Boldyrev, S. (2006), Spectrum of magnetohydrodynamic turbulence, *Phys. Rev. Lett.*, *96*, 115,002.

Borovsky, J. (2006), The flux-tube texture of the solar wind, *Eos. Trans. AGU*, *87*(52), Fall Meet. Abstr. SH43C-05.

Burlaga, L. F. (1995), *Interplanetary Magnetohydrodynamics*, Oxford Univ. Press, New York.

Burlaga, L. F., and K. W. Ogilvie (1973), Solar wind temperature and speed, *J. Geophys. Res.*, *78*, 2028.

Cho, J., and A. Lazarian (2003), Compressible magnetohydrodynamic turbulence: Mode coupling, scaling relations, anisotropy, viscosity-damped

regime and astrophysical implications, *Mon. Not. R. Astron. Soc.*, *345*, 325.
Cho, J., and E. T. Vishniac (2000), The anisotropy of magnetohydrodynamic Alfvénic turbulence, *Astrophys. J.*, *539*, 273.
Cho, J., A. Lazarian, and E. T. Vishniac (2002), Simulations of magnetohydrodynamic turbulence in a strongly magnetized medium, *Astrophys. J.*, *564*, 291.
Coleman, P. J. (1968), Turbulence, viscosity, and dissipation in the solar-wind plasma, *Astrophys. J.*, *153*, 371.
Daughton, W., and S. P. Gary (1998), Electromagnetic proton/proton instabilities in the solar wind, *J. Geophys. Res.*, *103*, 20,613.
Dmitruk, P., W. H. Matthaeus, L. J. Milano, S. Oughton, G. P. Zank, and D. J. Mullan (2002), Coronal heating distribution due to low-frequency, wave-driven turbulence, *Astrophys. J.*, *575*, 571.
Dobrowolny, M., A. Mangeney, and P. Veltri (1980), Fully developed anisotropic hydromagnetic turbulence in interplanetary space, *Phys. Rev. Lett.*, *45*, 144.
Feldman, W. C., J. R. Asbridge, S. J. Bame, and M. D. Montgomery (1973), On the origin of solar wind proton thermal anisotropy, *J. Geophys. Res.*, *78*, 6451.
Feldman, W. C., J. R. Asbridge, S. J. Bame, M. D. Montgomery, and S. P. Gary (1975), Solar wind electrons, *J. Geophys. Res.*, *80*, 4181.
Forman, M. A., and L. F. Burlaga (2003), Exploring the Castaing distribution function to study intermittence in the solar wind at L1, in *Solar Wind Ten*, edited by M. Velli, R. Bruno, and F. Malara, *AIP Conf. Proc.*, *679*, 554.
Freeman, J. W. (1988), Estimates of solar wind heating inside 0.3 AU, *Geophys. Res. Lett.*, *15*, 88.
Freeman, J. W., and R. E. Lopez (1985), The cold solar wind, *J. Geophys. Res.*, *90*, 9885.
Freeman, J. W., T. Totten, and S. Arya (1992), A determination of the polytropic index of the free streaming solar wind using improved temperature and density radial power-law indices, *EOS. Trans. AGU*, *73*, 238.
Galtier, S., S. V. Nazarenko, A. C. Newell, and A. Pouquet (2000), A weak turbulence theory for incompressible magnetohydrodynamics, *J. Plasma Phys.*, *63*, 447.
Galtier, S., S. V. Nazarenko, A. C. Newell, and A. Pouquet (2002), Anisotropic turbulence of shear-Alfvén waves, *Astrophys. J.*, *564*, L49.
Gazis, P. R. (1984), Observations of plasma bulk parameters and the energy balance of the solar wind between 1 and 10 AU, *J. Geophys. Res.*, *89*, 775.
Gazis, P. R., A. Barnes, J. D. Mihalov, and A. J. Lazarus (1994), Solar wind velocity and temperature in the outer heliosphere, *J. Geophys. Res.*, *99*, 6561.
Ghosh, S., W. H. Matthaeus, D. A. Roberts, and M. L. Goldstein (1998a), The evolution of slab fluctuations in the presence of pressure-balanced magnetic structures and velocity shears, *J. Geophys. Res.*, *103*, 23,691.
Ghosh, S., W. H. Matthaeus, D. A. Roberts, and M. L. Goldstein (1998b), Waves, structures, and the appearance of two-component turbulence in the solar wind, *J. Geophys. Res.*, *103*, 23,705.
Goldreich, P., and S. Sridhar (1995), Toward a theory of interstellar turbulence II. Strongly Alfvénic turbulence, *Astrophys. J.*, *438*, 763.
Goldstein, B. E., E. J. Smith, A. Balogh, T. S. Horbury, M. L. Goldstein, and D. A. Roberts (1995), Properties of magnetohydrodynamic turbulence in the solar wind as observed by Ulysses at high heliographic latitudes, *Geophys. Res. Lett.*, *22*, 3393.
Goldstein, M. L., D. A. Roberts, and C. A. Fitch (1994), Properties of the fluctuating magnetic helicity in the inertial and dissipation ranges of solar wind turbulence, *J. Geophys. Res.*, *99*, 11,519.
Grappin, R., A. Pouquet, and J. Léorat (1983), Dependence of MHD spectra on the velocity field-magnetic field correlation, *Astron. Astrophys.*, *126*, 51.
Grappin, R., A. Mangeney, and E. Marsch (1990), On the origin of solar wind MHD turbulence: Helios data revisited, *J. Geophys. Res.*, *95*, 8197.
Hamilton, K., C. W. Smith, and R. J. Leamon (2005), Dissipation range spectral characteristics at 1 AU, in *Solar Wind 11*, edited by B. Fleck and T. H. Zurbuchen, *ESA Spec. Publ.*, *ESA SP-592*, 547.
Haugen, N. E. L., A. Brandenburg, and W. Dobler (2004), Simulations of nonhelical hydromagnetic turbulence, *Phys. Rev. E.*, *70*, 016,308.
Hyesook, L., D. Ryu, J. Kim, T. W. Jones, and D. Balsara (2003), Numerical study of compressible magnetohydrodynamic turbulence in two dimensions, *Astrophys. J.*, *594*, 637.
Hollweg, J. V. (1981), The energy balance of the solar wind, in *The Sun as a Star*, edited by S. Jordan, *NASA Spec. Publ.*, *SP-450*, 355.
Hollweg, J. V. (1986), Transition region, corona, and solar wind in the coronal holes, *J. Geophys. Res.*, *91*, 4111.
Horbury, T. S., A. Balogh, R. J. Forsyth, and E. J. Smith (1996), Magnetic field signatures of unevolved turbulence in solar polar flows, *J. Geophys. Res.*, *101*, 405.
Iroshnikov, P. S. (1964), Turbulence of a conducting fluid in a strong magnetic field, *Sov. Astron.*, *7*, 566.
Isenberg, P. A. (2005), Turbulence-driven solar wind heating and energization of pickup protons in the outer heliosphere, *Astrophys. J.*, *623*, 502.
Kaghashvili, E. K., B. J. Vasquez, G. P. Zank, and J. V. Hollweg (2004), Deceleration of relative streaming between proton components among nonlinear low-frequency Alfvén waves, *J. Geophys. Res.*, *109*, A11105, doi:10.1029/2004JA010496.
Kinney, R. M., and J. C. MacWilliams (1998), Turbulent cascades in anisotropic magnetohydrodynamics, *Phys Rev. E*, *57*, 7111.
Kolmogorov, A. N. (1941), The local structure of turbulence in incompressible viscous fluid for very large Reynolds numbers, *Dokl. Akad. Nauk SSSR*, *30*, 301–305. (Reprinted in *Proc. R. Soc. London A*, *434*, 9–13, 1991.)
Kraichnan, R. H. (1965), Inertial-range spectrum of hydromagnetic turbulence, *Phys. Fluids*, *8*, 1385.
Krall, N. A., and A. W Trivelpiece (1973), *Principles of Plasma Physics*, McGraw-Hill, New York.
Leamon, R. J., C. W. Smith, N. F. Ness, W. H. Matthaeus, and H. K. Wong (1998a), Observational constraints on the dynamics of the interplanetary magnetic field dissipation range, *J. Geophys. Res.*, *103*, 4775.
Leamon, R. J., W. H. Matthaeus, C. W. Smith, and H. K. Wong (1998b), Contribution of cyclotron-resonant damping to kinetic dissipation of interplanetary turbulence, *Astrophys. J. Lett.*, *507*, 181.
Leamon, R. J., C. W. Smith, N. F. Ness, and H. K. Wong (1999), Dissipation range dynamics: Kinetic Alfvén waves and the importance of β_e, *J. Geophys. Res.*, *104*, 22,331.
Lie-Svendsen, Ø., and E. Leer (2000), The electron velocity distributions in the high-speed solar wind: Modeling the effects of protons, *J. Geophys. Res.*, *105*, 35.
Lithwick, Y., and P. Goldreich (2003), Imbalanced weak magnetohydrodynamic turbulence, *Astrophys. J.*, *582*, 1220.
Lithwick, Y., P. Goldreich, and S. Sridhar (2007), Imbalanced strong MHD turbulence, *Astrophys. J.*, *655*, 269.
Lopez, R. E., and J. W. Freeman (1986), Solar wind proton temperature-velocity relationship, *J. Geophys. Res.*, *91*, 1701. (Correction, *J. Geophys. Res.*, *92*, 13679, 1987.)
MacBride, B. T., M. A. Forman, and C. W. Smith (2005), Turbulence and the third moment of fluctuations: Kolmogorov's 4/5 law and its MHD analogues in the solar wind, in *Solar Wind 11*, edited by B. Fleck and T. H. Zurbuchen, *ESA Spec. Publ.*, *ESA SP-592*, 613.
Maron, J., and P. Goldreich (2001), Simulations of incompressible magnetohydrodynamic turbulence, *Astrophys. J.*, *554*, 1175.
Marsch, E., and A. K. Richter (1987), On the equation of state and collision time for a multicomponent, anisotropic solar wind, *Ann. Geophys.*, *5*, 71.
Marsch, E., K.-H. Mühlhäuser, R. Schwenn, H. Rosenbauer, W. Philipp, and F. M. Neubauer (1982), Solar wind protons: Three-dimensional velocity distributions and derived plasma parameters measured between 0.3 and 1 AU, *J. Geophys. Res.*, *87*, 52.
Marsch, E., K.-H. Mühlhäuser, H. Rosenbauer, and R. Schwenn (1983), On the equation of state of solar wind ions derived from Helios measurements, *J. Geophys. Res.*, *88*, 2982.
Matthaeus, W. H., and M. L. Goldstein (1982), Measurement of the rugged invariants of magnetohydrodynamic turbulence in the solar wind, *J. Geophys. Res.*, *87*, 6011.
Matthaeus, W. H., and Y. Zhou (1989), Extended inertial range phenomenology of magnetohydrodynamic turbulence, *Phys. Fluids B*, *1*, 1929.
Matthaeus, W. H., S. Ghosh, S. Oughton, and D. A. Roberts (1996), Anisotropic three-dimensional MHD turbulence, *J. Geophys. Res.*, *101*, 7619.
McComas, D. J., S. J. Bame, P. Barker, W. C. Feldman, J. L. Phillips, P. Riley, and J. W. Griffee (1998), Solar wind electron proton alpha monitor (SWEPAM) for the Advanced Composition Explorer, *Space Sci. Rev.*, *86*(1–4), 563.
McComas, D. J., B. L. Barraclough, H. O. Funsten, J. T. Gosling, E. Santiago-Muñoz, R. M. Skoug, B. E. Goldstein, M. Neugebauer, P. Riley, and A. Balogh (2000), Solar wind observations over Ulysses' first full polar orbit, *J. Geophys. Res.*, *105*, 10,419.
Müller, W.-C., and D. Biskamp (2000), Scaling properties of three-dimensional magnetohydrodynamic turbulence, *Phys. Rev. Lett.*, *84*, 475.
Müller, W.-C., D. Biskamp, and R. Grappin (2003), Statistical anisotropy of magnetohydrodynamic turbulence, *Phys. Rev. E*, *67*, 066,302.
Müller, W.-C., and R. Grappin (2005), Spectral energy dynamics in magnetohydrodynamic turbulence, *Phys. Rev. Lett.*, *95*, 114,502.
Neugebauer, M. (1981), Observations of the solar wind helium, *Fundam. Cosmic Phys.*, *7*, 131.
Neugebauer, M., and C. W. Snyder (1966), Mariner 2 observations of the solar wind: 1. Average properties, *J. Geophys. Res.*, *71*, 4469.

Newbury, J. A., C. T. Russell, J. L. Phillips, and S. P. Gary (1998), Electron temperature in the ambient solar wind: Typical properties and a lower bound at 1 AU, *J. Geophys. Res.*, *103*, 9553.

Ng, C. S., A. Bhattacharjee, and K. Germaschewski (2003), Anisotropic fluid turbulence in the interstellar medium and solar wind, *Phys.*, *10*, 1954.

Oughton, S., E. R. Priest, and W. H. Matthaeus (1994), The influence of a mean magnetic field on three-dimensional magnetohydrodynamic turbulence, *J. Fluid Mech.*, *280*, 95.

Oughton, S., P. Dmitruk, and W. H. Matthaeus (2003), Coronal heating and reduced MHD, in *Turbulence and Magnetic Fields in Astrophysics*, *Lect. Not. in Phys.*, vol. 614, edited by E. Falgarone and T. Passot, p. 28, Springer, New York.

Phillips, J. L., and J. T. Gosling (1990), Radial evolution of solar wind thermal electron distributions due to expansion and collisions, *J. Geophys. Res.*, *95*, 4217.

Phillips, J. L., J. T. Gosling, D. J. McComas, S. J. Bame, S. P. Gary, and E. J. Smith (1989), Anisotropic thermal electron distributions in the solar wind, *J. Geophys. Res.*, *94*, 6563.

Pilipp, W. G., H. Miggenrieder, K.-H. Mühläuser, H. Rosenbauer, and R. Schwenn (1990), Large-scale variations of thermal electron parameters in the solar wind between 0.3 and 1 AU, *J. Geophys. Res.*, *95*, 6305.

Pizzo, V., J. T. Gosling, A. J. Hundhausen, and S. J. Bame (1973), Large-scale dynamical effects upon the solar wind flow parameters, *J. Geophys. Res.*, *78*, 6469.

Podesta, J. J., D. A. Roberts, and M. L. Goldstein (2006), Power spectrum of small-scale turbulent velocity fluctuations in the solar wind, *J. Geophys. Res.*, *111*, A10109, doi:10.1029/2006JA011834.

Reisenfeld, D. B., et al. (2001), Helium energetics in the high-latitude solar wind: Ulysses observations, *J. Geophys. Res.*, *106*, 5693.

Richardson, J. D., J. W. Belcher, K. I. Paularena, and A. J. Lazarus (1995), Radial evolution of the solar wind from IMP 8 to Voyager 2, *Geophys. Res. Lett.*, *22*, 325.

Roberts, D. A., L. W. Klein, M. L. Goldstein, and W. H. Matthaeus (1987a), The nature and evolution of magnetohydrodynamic fluctuations in the solar wind: Voyager observations, *J. Geophys. Res.*, *92*, 11,021.

Roberts, D. A., M. L. Goldstein, L. W. Klein, and W. H. Matthaeus (1987b), Origin and evolution of fluctuations in the solar wind: Helios observations and Helios-Voyager comparisons, *J. Geophys. Res.*, *92*, 12,023.

Roberts, D. A., M. L. Goldstein, and L. W. Klein (1990), The amplitudes of interplanetary fluctuations: Stream structure, heliocentric distance, and frequency dependence, *J. Geophys. Res.*, *95*, 4203.

Schwartz, S. J., and E. Marsch (1983), The radial evolution of a single solar wind plasma parcel, *J. Geophys. Res.*, *88*, 9919.

Schwartz, S. J., W. C. Feldman, and S. P. Gary (1981), The source of proton anisotropy in the high-speed solar wind, *J. Geophys. Res.*, *86*, 541.

Schwenn, R. (1983), The "average" solar wind in the inner heliosphere: Structures and slow variations, in *Solar Wind Five*, *NASA Conf. Publ.*, *CP-2280*, 489.

Scime, E. E., S. J. Bame, W. C. Feldman, S. P. Gary, and J. L. Phillips (1994), Regulation of the solar wind electron heat flux from 1 to 5 AU: Ulysses observations, *J. Geophys. Res.*, *99*, 23,401.

Shebalin, J. V., W. H. Matthaeus, and D. Montgomery (1983), Anisotropy in MHD turbulence due to a mean magnetic field, *J. Plasma Phys.*, *29*, 525.

Smith, C. W., M. H. Acuña, L. F. Burlaga, J. L'Heureux, N. F. Ness, and J. Scheifele (1998), The ACE magnetic field experiment, *Space Sci. Rev.*, *86*(1–4), 613.

Smith, C. W., W. H. Matthaeus, G. P. Zank, N. F. Ness, S. Oughton, and J. D. Richardson (2001a), Heating of the low-latitude solar wind by dissipation of turbulent magnetic fluctuations, *J. Geophys. Res.*, *106*, 8253.

Smith, C. W., D. J. Mullan, N. F. Ness, R. M. Skoug, and J. Steinberg (2001b), Day the solar wind almost disappeared: Magnetic field fluctuations, wave refraction and dissipation, *J. Geophys. Res.*, *106*, 18,625.

Smith, C. W., D. J. Mullan, and N. F. Ness (2004), Further evidence of wave refraction associated with extended rarefaction events in the solar wind, *J. Geophys. Res.*, *109*, A01111, doi:10.1029/2003JA010113.

Smith, C. W., K. Hamilton, and B. J. Vasquez (2005), Variance Anisotropy in the Inertial range, in *Solar Wind 11*, edited by B. Fleck and T. H. Zurbuchen, *ESA Spec. Publ.*, *ESA SP-592*, 551.

Smith, C. W., B. J. Vasquez, and K. Hamilton (2006a), Interplanetary Magnetic Fluctuation Anisotropy in the Inertial Range, *J. Geophys. Res.*, *111*, A09111, doi:10.1029/2006JA011651.

Smith, C. W., K. Hamilton, B. J. Vasquez, and R. J. Leamon (2006b), Dependence of the dissipation range spectrum of interplanetary magnetic fluctuations upon the rate of energy cascade, *Astrophy. J.*, *645*, L85.

Smith, C. W., P. A. Isenberg, W. H. Matthaeus, and J. D. Richardson (2006c), Turbulent heating of the solar wind by newborn interstellar pickup protons, *Astrophy. J.*, *638*, 508.

Sreenivasan, K. R. (1995), On the universality of the Kolmogorov constant, *Phys. Fluids*, *7*, 2778.

Totten, T. L., J. W. Freeman, and S. Arya (1995), An empirical determination of the polytropic index for the free-streaming solar wind using Helios 1 data, *J. Geophys. Res.*, *100*, 13.

Tu, C.-Y. (1988), The damping of interplanetary Alfvénic fluctuations and the heating of the solar wind, *J. Geophys. Res.*, *93*, 7.

Tu, C.-Y., Z.-Y. Pu, and F.-S. Wei (1984), The power spectrum of interplanetary Alfvén fluctuations: Derivation of the governing equation and its solution, *J. Geophys. Res.*, *89*, 9695.

Velli, M. (2001), Hydrodynamics of the solar wind expansion, *Astrophys. Space Sci.*, *277*, 157.

Verma, M. K., D. A. Roberts, and M. L. Goldstein (1995), Turbulent heating and temperature evolution in the solar wind, *J. Geophys. Res.*, *100*, 19,839.

Verma, M. K., D. A. Roberts, M. L. Goldstein, S. Ghosh, and W. T. Stribling (1996), A numerical study of the nonlinear cascade of energy in magnetohydrodynamic turbulence, *J. Geophys. Res.*, *101*, 21,619.

Völk, H. J., and W. Alpers (1973), The propagation of Alfvén waves and their directional anisotropy in the solar wind, *Astrophys. Space Sci.*, *20*, 267.

Yeung, P. K., and Y. Zhou (1997), Universality of the Kolmgorov constant in numerical simulations of turbulence, *Phys. Rev. E*, *56*, 1746.

Zank, G. P., W. H. Matthaeus, and C. W. Smith (1996), Evolution of turbulent magnetic fluctuation power with heliospheric distance, *J. Geophys. Res.*, *101*, 17,093.

Zhou, Y., and W. H. Matthaeus (1990), Models of inertial range spectra of interplanetary magnetohydrodynamic turbulence, *J. Geophys. Res.*, *95*, 14,881.

K. Hamilton, B. T. MacBride, C. W. Smith, and B. J. Vasquez, Space Science Center, University of New Hampshire, Morse Hall, Durham, NH 03824, USA. (hamilton@briaxa.sr.unh.edu; btmb@cisunix.unh.edu; charles.smith@unh.edu; bernie.vasquez@unh.edu)

R. J. Leamon, ADNET Systems, Inc., NASA Goddard Space Flight Center, Code 671.1, Greenbelt, MD 20771, USA. (leamon@grace.nascom.nasa.gov)